Patni, M., Minera Rebulla, S., Groh, R., Pirrera, A., & Weaver, P. (2019). Efficient 3D Stress Capture of Variable-Stiffness and Sandwich Beam Structures. In *AIAA Scitech 2019 Forum, 7-11 January 2019, San Diego, California: Session: Composite Interlaminar Enhancement Methods and Modeling II* American Institute of Aeronautics and Astronautics Inc. (AIAA). https://doi.org/10.2514/6.2019-1763

Efficient 3D Stress Capture of Variable-Stiffness and Sandwich Beam Structures

M. Patni*, S. Minera†, R.M.J. Groh‡, A. Pirrera§ P.M. Weaver¶

Accurate modeling of composite structures is important for their safe application under different loading conditions. To provide accurate predictions of three-dimensional (3D) stress fields in an efficient computational framework, we employ a modeling approach that builds upon the recently developed hierarchical Serendipity Lagrange finite elements. The approach provides Layer-Wise (LW) and Equivalent Single-Layer (ESL) models for analyzing constant- and variable-stiffness laminated beam structures. To enhance the capability of the ESL model, two Zig-Zag (ZZ) functions, namely Murakami's ZZ function (MZZF) and the Refined ZZ theory function (RZT), are implemented. For constant-stiffness laminated and sandwich beams, the RZT ZZ function predicts the structural response more accurately than the MZZF. However, for variable-stiffness laminated structures, the applicability of RZT remains unknown and its accuracy is therefore tested within the present formulation. Results obtained are validated against 3D closed-form and 3D Finite Element (FE) solutions available from the literature. For similar levels of accuracy, significant gains in computational efficiency are achieved over 3D FE and LW models by using the ESL approach with RZT ZZ functions.

Nomenclature

A	=	cross-section area of the laminate
b	=	width of the laminate
$\bar{\boldsymbol{C}}$	=	material stiffness matrix
$\bar{C}_{ij}$	=	transformed elastic coefficients
$\mathcal{D}$	=	kinematic differential operator
E	=	Young's modulus
F_τ	=	cross-section expansion functions
G	=	shear modulus

*Marie Sklodowska-Curie Research Fellow, Bristol Composites Institute (ACCIS), University of Bristol, UK, Email: mayank.patni@bristol.ac.uk
†Marie Sklodowska-Curie Research Fellow, Bristol Composites Institute (ACCIS), University of Bristol, UK.
‡Royal Academy of Engineering Research Fellow, Bristol Composites Institute (ACCIS), University of Bristol, UK.
§Senior Lecturer in Composite Structures - EPSRC Research Fellow, Bristol Composites Institute (ACCIS), University of Bristol, UK.
¶Professor in Lightweight Structures, Bristol Composites Institute (ACCIS), University of Bristol, UK and Bernal Chair of Composite Materials and Structures, School of Engineering, University of Limerick, Castletroy, Ireland.

h	=	thickness of the laminate
k	=	layer number (lamina index)
$\boldsymbol{K}^{\tau sij}, \boldsymbol{K}^{\tau\varphi ij}, \boldsymbol{K}^{\phi sij}, \boldsymbol{K}^{\phi\varphi ij}$	=	Fundamental Nuclei of the stiffness matrix
L	=	length of the laminated beam
m	=	number of expansion terms
N_i	=	Lagrangian one-dimensional shape functions
N_l	=	number of layers
$\boldsymbol{u}$	=	displacement vector
u, v, w	=	displacement fields in x, y, z directions
$\boldsymbol{u}_{i\tau}$	=	generalized displacement vector
V	=	volume of the structure
$W_\mathrm{int}, W_\mathrm{ext}$	=	internal and external work
(x, y, z)	=	co-ordinates of the reference system
γ_{xz}, γ_{yz}	=	transverse shear strains
γ_{xy}	=	in-plane shear strain
δ	=	virtual variation
$\boldsymbol{\varepsilon}$	=	generalized strain vector
$\varepsilon_{xx}, \varepsilon_{yy}$	=	in-plane normal strains
ε_{zz}	=	transverse normal strain
θ	=	fiber orientation angle
ν	=	Poisson's ratio
$\boldsymbol{\sigma}$	=	generalized stress vector
σ_{xx}, σ_{yy}	=	in-plane normal stresses
σ_{zz}	=	transverse normal stress
τ_{xz}, τ_{yz}	=	transverse shear stresses
τ_{xy}	=	in-plane shear stress
ϕ^M	=	Murakami's zig-zag function
ϕ_x^R, ϕ_y^R	=	refined zig-zag theory functions
ψ_x, ϕ_y	=	zig-zag rotations about x and y axis

I. Introduction

The application of multi-layered composite structures has significantly increased in various engineering disciplines, including aerospace, automotive, sports and health. Laminated composites allow designers to tailor properties through-thickness by varying the fiber orientation of the plies within the laminate and optimizing the stacking sequence for structural performance. Recent advancements in composite manufacturing technology have facilitated the production of laminates with curvilinear fibers, so-called variable-stiffness (VS) composites (or Variable Angle Tow composites). This technological advance removes the constraint on fibers to be rectilinear within each lamina and provides scope for an enlarged design space. However, both types of composite laminate—with unidirectional and curvilinear fibers—lack reinforcement through the thickness and are prone to delamination failure, which adversely affects their structural integrity. Demanding levels of performance, especially in the aerospace industry, call for efficient modeling tools to predict the initiation of failure. To this end, models for accurate full-field stress prediction are an important prerequisite.

In modeling multi-layered composite and sandwich structures, major modeling challenges include: (i) predicting transverse shear and normal deformations occurring due to low orthotropy ratios (G_{13}/E_{11}) [1]; (ii) capturing the slope variation of the three displacement fields across the thickness due to transverse anisotropy, commonly known as the Zig-Zag (ZZ) effect [2]; and (iii) to account for the inter-laminar continuity (IC) of displacements and transverse stresses. In addition, modeling variable-stiffness laminates requires continuous path modeling to ensure continuity across the laminate [3]. Due to these aforementioned complexities, high-fidelity finite element models (FEM) or layer-wise (LW) theories are often employed to obtain reliable three-dimensional (3D) stresses with the desired level of accuracy. However, these models are computationally expensive and demand large amounts of computer storage. Thus, with the aim of developing computationally efficient design tools for the practicing engineer, there remains a need for efficient modeling techniques.

In Classical Laminate Theory (CLT) [4] and First-Order Shear Deformation Theory (FSDT) [5] composite layers are analyzed based on an equivalent single-layer description, which lacks the kinematic fidelity to accurately predict the 3D structural response of laminated composites. To overcome the deficiencies of CLT and FSDT, and to improve the stress prediction capacity of equivalent single-layer theories, several higher-order theories with enhanced kinematics have been proposed in the literature [6–9]. Local layer-wise functions (called zig-zag functions) have also been included within the global higher-order in-plane displacement approximation to account for the ZZ effect. The reader is referred to [10] for detailed historic review, and to [11] for most recent assessment of different zig-zag theories.

Out of various ZZ functions, Murakami's zig-zag Function (MZZF) [12] is widely employed by researchers. The MZZF is constructed by *a priori* assuming a periodic change of the displacement field slope at layer interfaces. Numerous studies [13–17] available in the literature adopt the concept of enhancing the displacement field with MZZF and have shown significant improvement in the accuracy with a marginal increase in the computational cost with respect to classical ESL models. However, the MZZF fails to predict accurate ply-level stresses when employed for sandwich

structures with large face-to-core stiffness ratios and thick laminates with arbitrary layup [18, 19]. As an alternative, the Refined Zig-Zag Theory (RZT) developed by Tessler *et al*. [20, 21] can be used. The RZT accounts for layer-wise differences in transverse shear moduli, which are the properties that physically drive the ZZ effect. Here, the differences in transverse shear rigidities of each layer, and the average transverse shear rigidities of the entire layup, define the layer-wise ZZ slopes of the in-plane displacement fields. Recent works [19, 22, 23] have shown the superiority of the RZT ZZ functions in capturing accurate ply level 3D stresses for straight-fiber laminated composites.

Most research in the literature focuses on modeling techniques for unidirectional laminated composite structures. These models need further enhancement in order to account for curvilinear fiber laminates, *i.e.* variable-stiffness (VS) composites. To date, most studies on VS laminates deal with global structural phenomena, *e.g.* vibration and buckling. For an extensive review of the literature, the interested reader is referred to [24]. Relatively little work has been conducted in capturing 3D stress fields in VS laminates. Out of these few works, most published papers on modeling VS laminates use finely meshed FE models that can be computationally prohibitive for rapid design iterations [25–27]. Tornabene *et al.* [28] evaluated the application of different structural theories on the static solution of doubly-curved variable-stiffness laminated composite panels and showed that accurate 3D stress fields for such laminates can only be predicted using layer-wise theories. In an attempt to develop more computationally efficient numerical models, Demasi *et al.* [29] formulated ESL models refined with MZZF and LW models based on the Generalized Unified Formulation (GUF) [30–32], and benchmarked the performance of the different approaches. However, the study mainly focused on highlighting the computational efficiency gains over 3D FE models. By validating relatively simple stacking sequences, the robustness of the approach in analyzing arbitrary and complex lay-ups remains an open question. Groh and Weaver [33, 34] describe a third-order zig-zag implementation based on RZT within a Hellinger-Reissner mixed variational framework and use it to predict 3D stresses for arbitrary VS laminates. This particular model was solved in the strong form using the Differential Quadrature Method, and because a global mesh was used, local singularities in the fiber definition caused noise in the numerical calculation of derivatives. Moreover, discrepancies in the transverse normal stresses for some laminates were observed when compared with 3D FE solutions. The authors' recent work on VS laminates [35] solves this disparity in the transverse stress results by adopting a LW model of the Serendipity Lagrange expansion (SLE) based Unified Formulation (UF). The LW approach of the displacement-based formulation was shown to yield accurate localized 3D stress fields. Although the model is computationally efficient compared to a 3D FE method, the LW approach is still prohibitive for preliminary design studies since the computational expense multiples with the number of layers.

In order to provide an efficient framework for modeling constant- and variable-stiffness laminates as well as sandwich structures, we propose an ESL approach implemented within the Serendipity Lagrange Expansion-based Unified Formulation (UF-SLE-ESL). The hierarchical capability of this expansion model provides significant versatility with respect to the structural modeling. To account for the through-thickness transverse anisotropy, MZZF and RZT ZZ

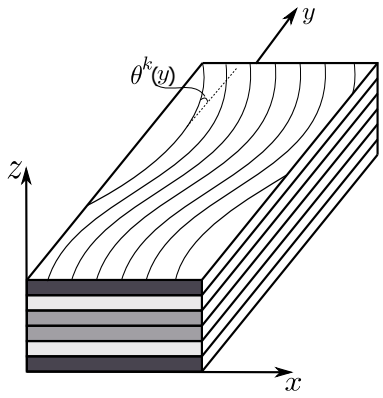

Fig. 1 Reference system for a variable-stiffness laminated beam.

functions are employed for the first time within the UF-SLE model. Since the formulation is displacement-based, it does not ensure continuous transverse stresses across layer interfaces. In order to capture through-thickness transverse shear and normal stresses reliably, a post-processing step is employed where the transverse stresses are recovered by integrating the in-plane stresses in Cauchy's 3D indefinite equilibrium equations.

The remainder of the paper is structured as follows. Section II A and B provides the displacement field approximation for LW, ESL-MZZF and ESL-RZT models within the Unified Formulation framework. Section II C, D and E provide an overview of the stiffness matrix, strain and stress computations, respectively. In Section III, results obtained using the present modeling approaches, for constant- and variable-stiffness laminates, are discussed and compared with 3D elasticity and 3D FE solutions. Finally, conclusions are drawn in Section IV.

II. Numerical Formulation

A. Displacement Field Approximation

Consider a variable-stiffness laminated beam of length L, rectangular cross-section of width b and thickness h, and composed of N_l layers. The material properties and the thickness of each layer may be entirely different. The beam is referred to in a Cartesian coordinate system (x, y, z), where the y-direction is defined to be along the principle beam axis, while the z-axis is in the transverse stacking direction as shown in Figure 1. Let θ denote the fiber angle measured with respect to the y-direction that can vary along the beam's span. Finally, let the superscript k be used to refer to layer number k.

Our model employs the Unified Formulation (UF) framework by Carrera and co-workers [36–38], which relies on a displacement-based formulation of the finite element method. The advantage of a finite element discretization is that arbitrary geometries and boundary conditions can readily be modeled. The three-dimensional displacement field is

given as

$$\boldsymbol{u}(x,y,z) = \{u \quad v \quad w\}^{\top}. \tag{1}$$

In the current setting, the longitudinal axis of the structure is discretized with four-noded, Lagrange 1D finite elements, so that the displacement field can be approximated element-wise by means of local shape functions $N_i(y)$, and generalized nodal displacements, $\boldsymbol{u}_i(x,z)$, such that

$$\boldsymbol{u}(x,y,z) = \sum_{i=1}^{4} N_i(y)\boldsymbol{u}_i(x,z). \tag{2}$$

The transverse, or cross-sectional, deformations are approximated using hierarchical Serendipity Lagrange Expansion (SLE) functions $F_\tau(x,z)$. Adopting this expansion model, cross-sections are discretized using four-noded Lagrange sub-domains and the displacement field within each sub-domain can be enriched by increasing the order of the local Serendipity Lagrange expansion. The cross-sectional displacement field at the i^{th} beam node is expressed as

$$\boldsymbol{u}_i(x,z) = \sum_{\tau=1}^{m} F_\tau(x,z)\boldsymbol{u}_{i\tau}, \tag{3}$$

where m is the number of terms depending on the order of expansion and $\boldsymbol{u}_{i\tau}$ are generalized displacement vectors. By introducing the cross-sectional approximation of Eq. (3) into the FE discretization along the beam axis of Eq. (2), the displacement field reads

$$\boldsymbol{u}(x,y,z) = \sum_{i=1}^{4}\sum_{\tau=1}^{m} N_i(y)F_\tau(x,z)\boldsymbol{u}_{i\tau}. \tag{4}$$

The reader is referred to [39, 40] for a more detailed implementation and treatment of SLE models.

B. Zig-Zag Kinematics

The UF-SLE model allows a LW approach to be implemented directly with each layer modeled as one sub-domain and the kinematics within each layer (or sub-domain) varied hierarchically. This representation allows for an accurate strain field by satisfying the ZZ requirement and an accurate determination of 3D stresses at layer level. However, the number of variables in the model scales with the number of layers in the laminate and thus, the added accuracy comes at greater computational cost. To overcome this issue, an ESL approach is implemented within the UF-SLE framework, *i.e.* a single 4−noded Serendipity Lagrange element is used to model the beam's cross-section. Thus, the number of unknowns in the model becomes independent of the number of layers. Furthermore, the hierarchical nature of the SLE function allows higher-order terms to be added in the displacement field to account for severe transverse shear and normal deformations. While the higher-order terms in the displacement field provide accurate modeling of global structural effects, they are not capable of explicitly capturing ZZ effects. Therefore, there is a need to incorporate ZZ kinematics within the ESL approach in order to present it as a good compromise between local, layer-wise accuracy and

computational cost. The most commonly used ZZ function is Murakami's ZZ function (MZZF) [12], which is given by

$$\phi^{M^k}(z) = (-1)^k \frac{2}{h^k}(z - z_m^k), \tag{5}$$

where z_m^k is the mid-plane coordinate and h^k is the thickness of layer k. MZZF assumes alternating values of $+1$ and -1 at the top and bottom interfaces regardless of the planar location. Also, it does not depend on the mechanical properties of layers and is often presented as an effective enrichment of the displacement field, regardless of the type of stacking sequence. Numerous studies in literature [14, 29] show that superior representation of displacements and stresses, combined with less computational cost, can be achieved by including MZZF for constant- and variable-stiffness laminates and sandwich structures. However, for symmetric (with more than three layers) and unsymmetric sandwich lay-ups, or for laminates with externally weak layers, MZZF fails to predict the stress response accurately [19]. Therefore, another class of zig-zag function, as introduced by Tessler *et al.* [20], termed Refined Zig-Zag Theory (RZT), is incorporated within the UF-SLE ESL model. In RZT, the zig-zag slopes m_i^k are defined by the difference between the transverse shear rigidities G_{iz}^k of layer k, and effective transverse shear rigidity G_i of the entire layup [23]

$$m_i^k = \frac{G_i}{G_{iz}^k} - 1, \qquad \text{with} \quad G_i = \left[\frac{1}{h}\sum_{k=1}^{N_l}\frac{h^k}{G_{iz}^k}\right]^{-1}, \quad i = x, y, \tag{6}$$

where N_l is the total number of layers, and h_k and h are the thickness of layer k and total laminate thickness, respectively. The ZZ function is defined by

$$\phi_i^{R^k}(z) = z m_i^k + c_i^k, \quad i = x, y \tag{7}$$

where c_i^k enforces interlaminar continuity and is given as

$$c_i^k = m_i^k \frac{h}{2} + \sum_{j=2}^{k} h^{j-1}\left(\frac{G_i}{G_{iz}^{j-1}} - \frac{G_i}{G_{iz}^k}\right). \tag{8}$$

It is to be noted that the RZT ZZ function $\phi_i^{R^k}(z)$ is derived from transverse material properties, therefore in case of variable-stiffness laminates, the function varies with the in-plane location, *i.e.* $\phi_i^{R^k}(x, y, z)$.

Following the standard definition of the MZZF and RZT ZZ functions, and incorporating these within the UF-SLE

framework, the assumed displacement field, as given by Eq. (4), can now be written:

$$
\begin{aligned}
u(x,y,z) &= \sum_{i=1}^{4} N_i(y)\left(\sum_{\tau=1}^{m} F_\tau(x,z)u_{i\tau} + \phi^M(z)\psi_{x_i}\right)\\
v(x,y,z) &= \sum_{i=1}^{4} N_i(y)\left(\sum_{\tau=1}^{m} F_\tau(x,z)v_{i\tau} + \phi^M(z)\psi_{y_i}\right)\\
w(x,y,z) &= \sum_{i=1}^{4} N_i(y)\left(\sum_{\tau=1}^{m} F_\tau(x,z)w_{i\tau}\right),
\end{aligned}
\tag{9}
$$

and

$$
\begin{aligned}
u(x,y,z) &= \sum_{i=1}^{4} N_i(y)\left(\sum_{\tau=1}^{m} F_\tau(x,z)u_{i\tau} + \phi_x^R(x,y,z)\psi_{x_i}\right)\\
v(x,y,z) &= \sum_{i=1}^{4} N_i(y)\left(\sum_{\tau=1}^{m} F_\tau(x,z)v_{i\tau} + \phi_y^R(x,y,z)\psi_{y_i}\right)\\
w(x,y,z) &= \sum_{i=1}^{4} N_i(y)\left(\sum_{\tau=1}^{m} F_\tau(x,z)w_{i\tau}\right),
\end{aligned}
\tag{10}
$$

where ψ_{x_i} and ψ_{y_i} are ZZ rotations at the i^{th} beam node. Finally, we now have three displacement field approximations in the UF-SLE model as given by Eqs. (4), (9) and (10) which correspond to the LW, the ESL-MZZF and the ESL-RZT theories, respectively. In the remainder of this paper, these models are referred as UF-LW, UF-MZZF and UF-RZT.

C. Fundamental Nucleus of the Stiffness Matrix

Elastic equilibrium is enforced via the Principle of Virtual Displacements, which, in a quasi-static setting, states that

$$
\delta W_{\text{int}} = \delta W_{\text{ext}}, \tag{11}
$$

where δ denotes the first variation with respect to displacements, and W_{int} and W_{ext} denote the internal and external work, respectively.

By definition, the internal work is the work done by the internal stresses over the corresponding internal strains and is equivalent to the elastic strain energy. Noting that $W_{\text{int}} = \sum_{\text{e}} W_{\text{int}}^{\text{e}}$ and letting l_{e} be the length of the generic beam element and A be the cross-sectional area,

$$
\delta W_{\text{int}}^{\text{e}} = \int_{l_{\text{e}}} \int_{A} \delta\boldsymbol{\varepsilon}^{\top}\boldsymbol{\sigma}\, dA\, dl. \tag{12}
$$

In the Unified Formulation notation, the internal work can be re-written as

$$
\delta W_{\text{int}}^{\text{e}} = \delta \boldsymbol{u}_{js\varphi}^{\top} \boldsymbol{K}_{\text{e}}^{\tau s\phi\varphi ij} \boldsymbol{u}_{i\tau\phi}, \tag{13}
$$

where

$$\boldsymbol{K}_{\mathrm{e}}^{\tau s \phi \varphi i j} = \begin{bmatrix} \boldsymbol{K}^{\tau s i j} & \boldsymbol{K}^{\tau \varphi i j} \\ \boldsymbol{K}^{\phi s i j} & \boldsymbol{K}^{\phi \varphi i j} \end{bmatrix}, \quad \boldsymbol{u}_{j s \varphi} = \begin{Bmatrix} u_{js} & v_{js} & w_{js} & \psi_{x_j} & \psi_{y_j} \end{Bmatrix}^{\top}, \quad \boldsymbol{u}_{i \tau \phi} = \begin{Bmatrix} u_{i\tau} & v_{i\tau} & w_{i\tau} & \psi_{x_i} & \psi_{y_i} \end{Bmatrix}^{\top}.$$

Matrices $\boldsymbol{K}^{\tau s i j}$, $\boldsymbol{K}^{\tau \varphi i j}$, $\boldsymbol{K}^{\phi s i j}$ and $\boldsymbol{K}^{\phi \varphi i j}$ are referred to as the *Fundamental Nuclei* of the stiffness matrix. For a given τ, s, i, j and ϕ, φ these matrices are of size 3×3, 3×2, 2×3 and 2×2, respectively. These *fundamental nuclei* are expanded by using the indices $\tau, s = 1, \ldots, m$; $\phi, \varphi = m + 1$ and $i, j = 1, \ldots, 4$; in order to obtain the elemental stiffness matrix, $\boldsymbol{K}_{\mathrm{e}}^{\tau s \phi \varphi i j}$. The layer-wise model is obtained by removing stiffness terms, $\boldsymbol{K}^{\tau \varphi i j}$, $\boldsymbol{K}^{\phi s i j}$ and $\boldsymbol{K}^{\phi \varphi i j}$, that account for the zig-zag kinematics. The explicit form for the matrix, $\boldsymbol{K}^{\tau s i j}$, can be found in Appendix A of [35] and the expression for other matrices, as required by ESL-ZZ models, are given as

$$\begin{aligned} K_{xx}^{\tau \varphi i j} = & < \bar{C}_{66}\, F_\tau \varphi_x^R N_{i,y} N_{j,y} > + < \bar{C}_{55}\, F_{\tau,z} \varphi_{x,z}^R N_i N_j > + < \bar{C}_{56}\, F_\tau \varphi_{x,z}^R N_{i,y} N_j > + < \bar{C}_{56}\, F_{\tau,z} \varphi_x^R N_i N_{j,y} > \\ & + < \bar{C}_{15}\, F_{\tau,z} \varphi_{x,x}^R N_i N_j > + < \bar{C}_{15}\, F_{\tau,x} \varphi_{x,z}^R N_i N_j > + < \bar{C}_{16}\, F_\tau \varphi_{x,x}^R N_{i,y} N_j > + < \bar{C}_{16}\, F_{\tau,x} \varphi_x^R N_i N_{j,y} > \\ & + < \bar{C}_{11}\, F_{\tau,x} \varphi_{x,x}^R N_i N_j > + < \bar{C}_{16}\, F_{\tau,x} \varphi_{x,y}^R N_i N_j > + < \bar{C}_{56}\, F_{\tau,z} \varphi_{x,y}^R N_i N_j > + < \bar{C}_{66}\, F_\tau \varphi_{x,y}^R N_{i,y} N_j >, \end{aligned} \tag{14}$$

$$\begin{aligned} K_{xy}^{\tau \varphi i j} = & < \bar{C}_{26}\, F_\tau \varphi_y^R N_{i,y} N_{j,y} > + < \bar{C}_{45}\, F_{\tau,z} \varphi_{y,z}^R N_i N_j > + < \bar{C}_{25}\, F_\tau \varphi_{y,z}^R N_{i,y} N_j > + < \bar{C}_{46}\, F_{\tau,z} \varphi_y^R N_i N_{j,y} > \\ & + < \bar{C}_{14}\, F_{\tau,z} \varphi_{y,x}^R N_i N_j > + < \bar{C}_{56}\, F_{\tau,x} \varphi_{y,z}^R N_i N_j > + < \bar{C}_{12}\, F_\tau \varphi_{y,x}^R N_{i,y} N_j > + < \bar{C}_{66}\, F_{\tau,x} \varphi_y^R N_i N_{j,y} > \\ & + < \bar{C}_{16}\, F_{\tau,x} \varphi_{y,x}^R N_i N_j > + < \bar{C}_{66}\, F_{\tau,x} \varphi_{y,y}^R N_i N_j > + < \bar{C}_{46}\, F_{\tau,z} \varphi_{y,y}^R N_i N_j > + < \bar{C}_{26}\, F_\tau \varphi_{y,y}^R N_{i,y} N_j >, \end{aligned} \tag{15}$$

$$\begin{aligned} K_{yx}^{\tau \varphi i j} = & < \bar{C}_{26}\, F_\tau \varphi_x^R N_{i,y} N_{j,y} > + < \bar{C}_{45}\, F_{\tau,z} \varphi_{x,z}^R N_i N_j > + < \bar{C}_{46}\, F_\tau \varphi_{x,z}^R N_{i,y} N_j > + < \bar{C}_{25}\, F_{\tau,z} \varphi_x^R N_i N_{j,y} > \\ & + < \bar{C}_{56}\, F_{\tau,z} \varphi_{x,x}^R N_i N_j > + < \bar{C}_{14}\, F_{\tau,x} \varphi_{x,z}^R N_i N_j > + < \bar{C}_{66}\, F_\tau \varphi_{x,x}^R N_{i,y} N_j > + < \bar{C}_{12}\, F_{\tau,x} \varphi_x^R N_i N_{j,y} > \\ & + < \bar{C}_{16}\, F_{\tau,x} \varphi_{x,x}^R N_i N_j > + < \bar{C}_{12}\, F_{\tau,x} \varphi_{x,y}^R N_i N_j > + < \bar{C}_{25}\, F_{\tau,z} \varphi_{x,y}^R N_i N_j > + < \bar{C}_{26}\, F_\tau \varphi_{x,y}^R N_{i,y} N_j >, \end{aligned} \tag{16}$$

$$\begin{aligned} K_{yy}^{\tau \varphi i j} = & < \bar{C}_{22}\, F_\tau \varphi_y^R N_{i,y} N_{j,y} > + < \bar{C}_{44}\, F_{\tau,z} \varphi_{y,z}^R N_i N_j > + < \bar{C}_{24}\, F_\tau \varphi_{y,z}^R N_{i,y} N_j > + < \bar{C}_{24}\, F_{\tau,z} \varphi_y^R N_i N_{j,y} > \\ & + < \bar{C}_{46}\, F_{\tau,z} \varphi_{y,x}^R N_i N_j > + < \bar{C}_{46}\, F_{\tau,x} \varphi_{y,z}^R N_i N_j > + < \bar{C}_{26}\, F_\tau \varphi_{y,x}^R N_{i,y} N_j > + < \bar{C}_{26}\, F_{\tau,x} \varphi_y^R N_i N_{j,y} > \\ & + < \bar{C}_{66}\, F_{\tau,x} \varphi_{y,x}^R N_i N_j > + < \bar{C}_{26}\, F_{\tau,x} \varphi_{y,y}^R N_i N_j > + < \bar{C}_{24}\, F_{\tau,z} \varphi_{y,y}^R N_i N_j > + < \bar{C}_{22}\, F_\tau \varphi_{y,y}^R N_{i,y} N_j >, \end{aligned} \tag{17}$$

$$\begin{aligned} K_{zx}^{\tau \varphi i j} = & < \bar{C}_{46}\, F_\tau \varphi_x^R N_{i,y} N_{j,y} > + < \bar{C}_{35}\, F_{\tau,z} \varphi_{x,z}^R N_i N_j > + < \bar{C}_{36}\, F_\tau \varphi_{x,z}^R N_{i,y} N_j > + < \bar{C}_{45}\, F_{\tau,z} \varphi_x^R N_i N_{j,y} > \\ & + < \bar{C}_{55}\, F_{\tau,z} \varphi_{x,x}^R N_i N_j > + < \bar{C}_{13}\, F_{\tau,x} \varphi_{x,z}^R N_i N_j > + < \bar{C}_{56}\, F_\tau \varphi_{x,x}^R N_{i,y} N_j > + < \bar{C}_{14}\, F_{\tau,x} \varphi_x^R N_i N_{j,y} > \\ & + < \bar{C}_{15}\, F_{\tau,x} \varphi_{x,x}^R N_i N_j > + < \bar{C}_{14}\, F_{\tau,x} \varphi_{x,y}^R N_i N_j > + < \bar{C}_{45}\, F_{\tau,z} \varphi_{x,y}^R N_i N_j > + < \bar{C}_{46}\, F_\tau \varphi_{x,y}^R N_{i,y} N_j >, \end{aligned} \tag{18}$$

$$K_{zy}^{\tau\varphi ij} = < \bar{C}_{24}\ F_\tau \varphi_y^R N_{i,y} N_{j,y} > + < \bar{C}_{34}\ F_{\tau,z} \varphi_{y,z}^R N_i N_j > + < \bar{C}_{23}\ F_\tau \varphi_{y,z}^R N_{i,y} N_j > + < \bar{C}_{44}\ F_{\tau,z} \varphi_y^R N_i N_{j,y} >$$
$$+ < \bar{C}_{45}\ F_{\tau,z} \varphi_{y,x}^R N_i N_j > + < \bar{C}_{36}\ F_{\tau,x} \varphi_{y,z}^R N_i N_j > + < \bar{C}_{25}\ F_\tau \varphi_{y,x}^R N_{i,y} N_j > + < \bar{C}_{46}\ F_{\tau,x} \varphi_y^R N_i N_{j,y} > \quad (19)$$
$$+ < \bar{C}_{56}\ F_{\tau,x} \varphi_{y,x}^R N_i N_j > + < \bar{C}_{46}\ F_{\tau,x} \varphi_{y,y}^R N_i N_j > + < \bar{C}_{44}\ F_{\tau,z} \varphi_{y,y}^R N_i N_j > + < \bar{C}_{24}\ F_\tau \varphi_{y,y}^R N_{i,y} N_j >,$$

$$K_{xx}^{\phi sij} = < \bar{C}_{66}\ \phi_x^R F_s N_{i,y} N_{j,y} > + < \bar{C}_{55}\ \phi_{x,z}^R F_{s,z} N_i N_j > + < \bar{C}_{56}\ \phi_x^R F_{s,z} N_{i,y} N_j > + < \bar{C}_{56}\ \phi_{x,z}^R F_s N_i N_{j,y} >$$
$$+ < \bar{C}_{15}\ \phi_{x,z}^R F_{s,x} N_i N_j > + < \bar{C}_{15}\ \phi_{x,x}^R F_{s,z} N_i N_j > + < \bar{C}_{16}\ \phi_x^R F_{s,x} N_{i,y} N_j > + < \bar{C}_{16}\ \phi_{x,x}^R F_s N_i N_{j,y} > \quad (20)$$
$$+ < \bar{C}_{11}\ \phi_{x,x}^R F_{s,x} N_i N_j > + < \bar{C}_{16}\ \phi_{x,y}^R F_{s,x} N_i N_j > + < \bar{C}_{56}\ \phi_{x,y}^R F_{s,z} N_i N_j > + < \bar{C}_{66}\ \phi_{x,y}^R F_s N_i N_{j,y} >,$$

$$K_{xy}^{\phi sij} = < \bar{C}_{26}\ \phi_x^R F_s N_{i,y} N_{j,y} > + < \bar{C}_{45}\ \phi_{x,z}^R F_{s,z} N_i N_j > + < \bar{C}_{25}\ \phi_x^R F_{s,z} N_{i,y} N_j > + < \bar{C}_{46}\ \phi_{x,z}^R F_s N_i N_{j,y} >$$
$$+ < \bar{C}_{14}\ \phi_{x,z}^R F_{s,x} N_i N_j > + < \bar{C}_{56}\ \phi_{x,x}^R F_{s,z} N_i N_j > + < \bar{C}_{12}\ \phi_x^R F_{s,x} N_{i,y} N_j > + < \bar{C}_{66}\ \phi_{x,x}^R F_s N_i N_{j,y} > \quad (21)$$
$$+ < \bar{C}_{16}\ \phi_{x,x}^R F_{s,x} N_i N_j > + < \bar{C}_{12}\ \phi_{x,y}^R F_{s,x} N_i N_j > + < \bar{C}_{25}\ \phi_{x,y}^R F_{s,z} N_i N_j > + < \bar{C}_{26}\ \phi_{x,y}^R F_s N_i N_{j,y} >,$$

$$K_{xz}^{\phi sij} = < \bar{C}_{46}\ \phi_x^R F_s N_{i,y} N_{j,y} > + < \bar{C}_{35}\ \phi_{x,z}^R F_{s,z} N_i N_j > + < \bar{C}_{45}\ \phi_x^R F_{s,z} N_{i,y} N_j > + < \bar{C}_{36}\ \phi_{x,z}^R F_s N_i N_{j,y} >$$
$$+ < \bar{C}_{13}\ \phi_{x,z}^R F_{s,x} N_i N_j > + < \bar{C}_{55}\ \phi_{x,x}^R F_{s,z} N_i N_j > + < \bar{C}_{14}\ \phi_x^R F_{s,x} N_{i,y} N_j > + < \bar{C}_{56}\ \phi_{x,x}^R F_s N_i N_{j,y} > \quad (22)$$
$$+ < \bar{C}_{15}\ \phi_{x,x}^R F_{s,x} N_i N_j > + < \bar{C}_{14}\ \phi_{x,y}^R F_{s,x} N_i N_j > + < \bar{C}_{45}\ \phi_{x,y}^R F_{s,z} N_i N_j > + < \bar{C}_{46}\ \phi_{x,y}^R F_s N_i N_{j,y} >,$$

$$K_{yx}^{\phi sij} = < \bar{C}_{26}\ \phi_y^R F_s N_{i,y} N_{j,y} > + < \bar{C}_{45}\ \phi_{y,z}^R F_{s,z} N_i N_j > + < \bar{C}_{46}\ \phi_y^R F_{s,z} N_{i,y} N_j > + < \bar{C}_{25}\ \phi_{y,z}^R F_s N_i N_{j,y} >$$
$$+ < \bar{C}_{56}\ \phi_{y,z}^R F_{s,x} N_i N_j > + < \bar{C}_{14}\ \phi_{y,x}^R F_{s,z} N_i N_j > + < \bar{C}_{66}\ \phi_y^R F_{s,x} N_{i,y} N_j > + < \bar{C}_{12}\ \phi_{y,x}^R F_s N_i N_{j,y} > \quad (23)$$
$$+ < \bar{C}_{16}\ \phi_{y,x}^R F_{s,x} N_i N_j > + < \bar{C}_{66}\ \phi_{y,y}^R F_{s,x} N_i N_j > + < \bar{C}_{46}\ \phi_{y,y}^R F_{s,z} N_i N_j > + < \bar{C}_{26}\ \phi_{y,y}^R F_s N_i N_{j,y} >,$$

$$K_{yy}^{\phi sij} = < \bar{C}_{22}\ \phi_y^R F_s N_{i,y} N_{j,y} > + < \bar{C}_{44}\ \phi_{y,z}^R F_{s,z} N_i N_j > + < \bar{C}_{24}\ \phi_y^R F_{s,z} N_{i,y} N_j > + < \bar{C}_{24}\ \phi_{y,z}^R F_s N_i N_{j,y} >$$
$$+ < \bar{C}_{46}\ \phi_{y,z}^R F_{s,x} N_i N_j > + < \bar{C}_{46}\ \phi_{y,x}^R F_{s,z} N_i N_j > + < \bar{C}_{26}\ \phi_y^R F_{s,x} N_{i,y} N_j > + < \bar{C}_{26}\ \phi_{y,x}^R F_s N_i N_{j,y} > \quad (24)$$
$$+ < \bar{C}_{66}\ \phi_{y,x}^R F_{s,x} N_i N_j > + < \bar{C}_{26}\ \phi_{y,y}^R F_{s,x} N_i N_j > + < \bar{C}_{24}\ \phi_{y,y}^R F_{s,z} N_i N_j > + < \bar{C}_{22}\ \phi_{y,y}^R F_s N_i N_{j,y} >,$$

$$K_{yz}^{\phi sij} = < \bar{C}_{24}\ \phi_y^R F_s N_{i,y} N_{j,y} > + < \bar{C}_{34}\ \phi_{y,z}^R F_{s,z} N_i N_j > + < \bar{C}_{44}\ \phi_y^R F_{s,z} N_{i,y} N_j > + < \bar{C}_{23}\ \phi_{y,z}^R F_s N_i N_{j,y} >$$
$$+ < \bar{C}_{36}\ \phi_{y,z}^R F_{s,x} N_i N_j > + < \bar{C}_{45}\ \phi_{y,x}^R F_{s,z} N_i N_j > + < \bar{C}_{46}\ \phi_y^R F_{s,x} N_{i,y} N_j > + < \bar{C}_{25}\ \phi_{y,x}^R F_s N_i N_{j,y} > \quad (25)$$
$$+ < \bar{C}_{56}\ \phi_{y,x}^R F_{s,x} N_i N_j > + < \bar{C}_{46}\ \phi_{y,y}^R F_{s,x} N_i N_j > + < \bar{C}_{44}\ \phi_{y,y}^R F_{s,z} N_i N_j > + < \bar{C}_{24}\ \phi_{y,y}^R F_s N_i N_{j,y} >,$$

$$K_{xx}^{\phi\varphi ij} = < \bar{C}_{66}\ \phi_x^R \varphi_x^R N_{i,y} N_{j,y} > + < \bar{C}_{55}\ \phi_{x,z}^R \varphi_{x,z}^R N_i N_j > + < \bar{C}_{56}\ \phi_x^R \varphi_{x,z}^R N_{i,y} N_j > + < \bar{C}_{56}\ \phi_{x,z}^R \varphi_x^R N_i N_{j,y} >$$
$$+ < \bar{C}_{15}\ \phi_{x,z}^R \varphi_{x,x}^R N_i N_j > + < \bar{C}_{15}\ \phi_{x,x}^R \varphi_{x,z}^R N_i N_j > + < \bar{C}_{16}\ \phi_x^R \varphi_{x,x}^R N_{i,y} N_j > + < \bar{C}_{16}\ \phi_{x,x}^R \varphi_x^R N_i N_{j,y} > \quad (26)$$
$$+ < \bar{C}_{11}\ \phi_{x,x}^R \varphi_{x,x}^R N_i N_j > + < \bar{C}_{16}\ \phi_{x,x}^R \varphi_{x,y}^R N_i N_j > + < \bar{C}_{16}\ \phi_{x,y}^R \varphi_{x,x}^R N_i N_j > + < \bar{C}_{56}\ \phi_{x,y}^R \varphi_{x,z}^R N_i N_j >$$
$$+ < \bar{C}_{56}\ \phi_{x,z}^R \varphi_{x,y}^R N_i N_j > + < \bar{C}_{66}\ \phi_{x,y}^R \varphi_{x,y}^R N_i N_j > + < \bar{C}_{66}\ \phi_x^R \varphi_{x,y}^R N_{i,y} N_j > + < \bar{C}_{66}\ \phi_{x,y}^R \varphi_x^R N_i N_{j,y} >,$$

$$
\begin{aligned}
K_{xy}^{\phi\varphi ij} = & < \bar{C}_{26}\ \phi_x^R \varphi_y^R N_{i,y} N_{j,y} > + < \bar{C}_{45}\ \phi_{x,z}^R \varphi_{y,z}^R N_i N_j > + < \bar{C}_{25}\ \phi_x^R \varphi_{y,z}^R N_{i,y} N_j > + < \bar{C}_{46}\ \phi_{x,z}^R \varphi_y^R N_i N_{j,y} > \\
& + < \bar{C}_{14}\ \phi_{x,z}^R \varphi_{y,x}^R N_i N_j > + < \bar{C}_{56}\ \phi_{x,x}^R \varphi_{y,z}^R N_i N_j > + < \bar{C}_{12}\ \phi_x^R \varphi_{y,x}^R N_{i,y} N_j > + < \bar{C}_{66}\ \phi_{x,x}^R \varphi_y^R N_i N_{j,y} > \\
& + < \bar{C}_{16}\ \phi_{x,x}^R \varphi_{y,x}^R N_i N_j > + < \bar{C}_{66}\ \phi_{x,x}^R \varphi_{y,y}^R N_i N_j > + < \bar{C}_{12}\ \phi_{x,y}^R \varphi_{y,x}^R N_i N_j > + < \bar{C}_{25}\ \phi_{x,y}^R \varphi_{y,z}^R N_i N_j > \\
& + < \bar{C}_{46}\ \phi_{x,z}^R \varphi_{y,y}^R N_i N_j > + < \bar{C}_{26}\ \phi_{x,y}^R \varphi_{y,y}^R N_i N_j > + < \bar{C}_{26}\ \phi_x^R \varphi_{y,y}^R N_{i,y} N_j > + < \bar{C}_{26}\ \phi_{x,y}^R \varphi_y^R N_i N_{j,y} >,
\end{aligned}
\tag{27}
$$

$$
\begin{aligned}
K_{yx}^{\phi\varphi ij} = & < \bar{C}_{26}\ \phi_y^R \varphi_x^R N_{i,y} N_{j,y} > + < \bar{C}_{45}\ \phi_{y,z}^R \varphi_{x,z}^R N_i N_j > + < \bar{C}_{46}\ \phi_y^R \varphi_{x,z}^R N_{i,y} N_j > + < \bar{C}_{25}\ \phi_{y,z}^R \varphi_x^R N_i N_{j,y} > \\
& + < \bar{C}_{56}\ \phi_{y,z}^R \varphi_{x,x}^R N_i N_j > + < \bar{C}_{14}\ \phi_{y,x}^R \varphi_{x,z}^R N_i N_j > + < \bar{C}_{66}\ \phi_y^R \varphi_{x,x}^R N_{i,y} N_j > + < \bar{C}_{12}\ \phi_{y,x}^R \varphi_x^R N_i N_{j,y} > \\
& + < \bar{C}_{16}\ \phi_{y,x}^R \varphi_{x,x}^R N_i N_j > + < \bar{C}_{12}\ \phi_{y,x}^R \varphi_{x,y}^R N_i N_j > + < \bar{C}_{66}\ \phi_{y,y}^R \varphi_{x,x}^R N_i N_j > + < \bar{C}_{46}\ \phi_{y,y}^R \varphi_{x,z}^R N_i N_j > \\
& + < \bar{C}_{25}\ \phi_{y,z}^R \varphi_{x,y}^R N_i N_j > + < \bar{C}_{26}\ \phi_{y,y}^R \varphi_{x,y}^R N_i N_j > + < \bar{C}_{26}\ \phi_y^R \varphi_{x,y}^R N_{i,y} N_j > + < \bar{C}_{26}\ \phi_{y,y}^R \varphi_x^R N_i N_{j,y} >,
\end{aligned}
\tag{28}
$$

$$
\begin{aligned}
K_{yy}^{\phi\varphi ij} = & < \bar{C}_{22}\ \phi_y^R \varphi_y^R N_{i,y} N_{j,y} > + < \bar{C}_{44}\ \phi_{y,z}^R \varphi_{y,z}^R N_i N_j > + < \bar{C}_{24}\ \phi_y^R \varphi_{y,z}^R N_{i,y} N_j > + < \bar{C}_{24}\ \phi_{y,z}^R \varphi_y^R N_i N_{j,y} > \\
& + < \bar{C}_{46}\ \phi_{y,z}^R \varphi_{y,x}^R N_i N_j > + < \bar{C}_{46}\ \phi_{y,x}^R \varphi_{y,z}^R N_i N_j > + < \bar{C}_{26}\ \phi_y^R \varphi_{y,x}^R N_{i,y} N_j > + < \bar{C}_{26}\ \phi_{y,x}^R \varphi_y^R N_i N_{j,y} > \\
& + < \bar{C}_{66}\ \phi_{y,x}^R \varphi_{y,x}^R N_i N_j > + < \bar{C}_{26}\ \phi_{y,x}^R \varphi_{y,y}^R N_i N_j > + < \bar{C}_{26}\ \phi_{y,y}^R \varphi_{y,x}^R N_i N_j > + < \bar{C}_{24}\ \phi_{y,y}^R \varphi_{y,z}^R N_i N_j > \\
& + < \bar{C}_{24}\ \phi_{y,z}^R \varphi_{y,y}^R N_i N_j > + < \bar{C}_{22}\ \phi_{y,y}^R \varphi_{y,y}^R N_i N_j > + < \bar{C}_{22}\ \phi_y^R \varphi_{y,y}^R N_{i,y} N_j > + < \bar{C}_{22}\ \phi_{y,y}^R \varphi_y^R N_i N_{j,y} >,
\end{aligned}
\tag{29}
$$

where $< (.) >= \int_V (.)\, dV$, calculated using Gaussian quadrature, and $\bar{C}_{ij}$ are the material stiffness coefficients as discussed in Section D. The above expressions are applicable for the UF-RZT model. The stiffness matrix for the UF-MZZF model can be calculated by replacing ϕ_x^R and ϕ_y^R by ϕ^M and its variation φ_x^R and φ_y^R by φ^M in Eqs. (14)–(29). The elemental stiffness matrix, so-obtained, is assembled in a global stiffness matrix following the standard finite element procedure. For the sake of brevity, the derivation of the fundamental nucleus of the loading vector from the virtual variation of the external work is not reported here, but can be found in [36].

D. Strain and Stress Components

From basic elasticity, the generalized strain component vector can be written as

$$
\boldsymbol{\varepsilon} = \mathcal{D}\boldsymbol{u}, \tag{30}
$$

where $\boldsymbol{\varepsilon}^\top = \left\{\varepsilon_{xx}, \varepsilon_{yy}, \varepsilon_{zz}, \gamma_{yz}, \gamma_{zx}, \gamma_{xy}\right\}$ and $\mathcal{D}$ is the kinematic partial differential operator

$$
\mathcal{D} = \begin{bmatrix}
\frac{\partial}{\partial x} & 0 & 0 & 0 & \frac{\partial}{\partial z} & \frac{\partial}{\partial y} \\
0 & \frac{\partial}{\partial y} & 0 & \frac{\partial}{\partial z} & 0 & \frac{\partial}{\partial x} \\
0 & 0 & \frac{\partial}{\partial z} & \frac{\partial}{\partial y} & \frac{\partial}{\partial x} & 0
\end{bmatrix}^\top . \tag{31}
$$

By substituting Eqs. (4), (9) and (10), in Eq. (30), the elemental strain component vector for UF-LW, UF-MZZF and UF-RZT models is given by

$$\boldsymbol{\varepsilon} = \boldsymbol{G}_{i\tau}\boldsymbol{u}_{i\tau}, \quad \boldsymbol{\varepsilon} = \boldsymbol{G}_{i\tau}\boldsymbol{u}_{i\tau} + \boldsymbol{G}_i^M\boldsymbol{\psi}_i, \quad \text{and} \quad \boldsymbol{\varepsilon} = \boldsymbol{G}_{i\tau}\boldsymbol{u}_{i\tau} + \boldsymbol{G}_i^R\boldsymbol{\psi}_i, \tag{32}$$

respectively, where

$$\boldsymbol{G}_{i\tau} = \begin{bmatrix} N_i F_{\tau,x} & 0 & 0 \\ 0 & N_{i,y} F_\tau & 0 \\ 0 & 0 & N_i F_{\tau,z} \\ 0 & N_i F_{\tau,z} & N_{i,y} F_\tau \\ N_i F_{\tau,z} & 0 & N_i F_{\tau,x} \\ N_{i,y} F_\tau & N_i F_{\tau,x} & 0 \end{bmatrix}, \quad \boldsymbol{u}_{i\tau} = \begin{Bmatrix} u_{i\tau} \\ v_{i\tau} \\ w_{i\tau} \end{Bmatrix},$$

$$\boldsymbol{G}_i^M = \begin{bmatrix} 0 & 0 & 0 \\ 0 & 0 & 0 \\ 0 & 0 & 0 \\ 0 & N_i\phi^M_{,z} & 0 \\ N_i\phi^M_{,z} & 0 & 0 \\ 0 & 0 & 0 \end{bmatrix}, \quad \boldsymbol{G}_i^R = \begin{bmatrix} N_i\phi^R_{x,x} & 0 & 0 \\ 0 & N_i\phi^R_{y,y} + N_{i,y}\phi^R_y & 0 \\ 0 & 0 & 0 \\ 0 & N_i\phi^R_{y,z} & 0 \\ N_i\phi^R_{x,z} & 0 & 0 \\ N_i\phi^R_{x,y} + N_{i,y}\phi^R_x & N_i\phi^R_{y,x} & 0 \end{bmatrix}, \quad \boldsymbol{\psi}_i = \begin{Bmatrix} \psi_{x_i} \\ \psi_{y_i} \\ 0 \end{Bmatrix}.$$

Eqs. (32) use Einstein's summation notation over repeated indices and a subscript preceded by a comma denotes differentiation with respect to the corresponding spatial coordinate. It is noted that in case of constant-stiffness (straight fiber) laminate, the RZT ZZ functions depend only on the thickness coordinate, and therefore, derivatives of ϕ_x^R and ϕ_y^R with respect to x and y are zero. Furthermore, in the present study, we have considered variable-stiffness laminates with fiber-angle variation only along the spanwise direction y, and thus, $\phi^R_{x,x}$ and $\phi^R_{y,x}$ are zero.

For a linear elastic material undergoing infinitesimal strains and small displacements, the stresses are derived from the constitutive relation as given below,

$$\boldsymbol{\sigma} = \bar{\boldsymbol{C}}\boldsymbol{\varepsilon}, \tag{33}$$

or

$$\begin{Bmatrix} \sigma_{xx} \\ \sigma_{yy} \\ \sigma_{zz} \\ \tau_{yz} \\ \tau_{xz} \\ \tau_{xy} \end{Bmatrix} = \begin{bmatrix} \bar{C}_{11} & \bar{C}_{12} & \bar{C}_{13} & \bar{C}_{14} & \bar{C}_{15} & \bar{C}_{16} \\ & \bar{C}_{22} & \bar{C}_{23} & \bar{C}_{24} & \bar{C}_{25} & \bar{C}_{26} \\ & & \bar{C}_{33} & \bar{C}_{34} & \bar{C}_{35} & \bar{C}_{36} \\ & & & \bar{C}_{44} & \bar{C}_{45} & \bar{C}_{46} \\ & Symmetric & & & \bar{C}_{55} & \bar{C}_{56} \\ & & & & & \bar{C}_{66} \end{bmatrix} \begin{Bmatrix} \varepsilon_{xx} \\ \varepsilon_{yy} \\ \varepsilon_{zz} \\ \gamma_{yz} \\ \gamma_{xz} \\ \gamma_{xy} \end{Bmatrix}, \tag{34}$$

where coefficients $\bar{C}_{ij}$ are the transformed elastic coefficients referred to the global (x, y, z) coordinate system that depends on the mechanical properties of the laminate material and fiber orientation angle. The explicit expression for coefficients C_{ij}^{k} are not included here for sake of brevity, but can be found in [41].

E. Posteriori Calculation of the Transverse Stresses

As the present approach is displacement-based, computing stresses using the constitutive relation may lead to discontinuities in the transverse stresses at the interface between two adjacent layers, thereby violating traction continuity. Accurate modeling of a laminated structure requires a description of inter-laminar continuous transverse stresses. Therefore, in the current model transverse stresses are recovered by employing the indefinite equilibrium equations of 3D elasticity and integrating in-plane stresses in the thickness direction. The 3D stress equilibrium equations for the static case, and in the absence of body forces, are

$$\sigma_{ij_{,j}} = 0, \quad i, j = x, y, z, \tag{35}$$

where a comma denotes differentiation and Einstein's summation notation has been used. In summary, the in-plane stresses, σ_{xx}, σ_{yy} and τ_{xy}, are computed conventionally using the constitutive relations. Transverse shear and normal stresses, τ_{xz}, τ_{yz}, and σ_{zz} are calculated as

$$\sigma_{iz}^{k}(z) = \sigma_{iz_b}^{k} - \int_{z_b^k}^{z} \left(\sigma_{ix_{,x}} + \sigma_{iy_{,y}} \right) dz, \tag{36}$$

where $\sigma_{iz}^{k}(z)$ is the stress in the k^{th}-layer and $\sigma_{iz_b}^{k}$ is the stress at the bottom of the k^{th}-layer. This technique is commonly known as Stress Recovery (SR). Additionally, the hierarchical nature of the UF-SLE model allows for higher-order terms in the displacement field approximation to be used, and therefore, derivatives of in-plane stresses can be computed analytically. On the other hand, in classic 3D FE elements, linear or quadratic elements are usually employed, and thus, the derivatives of in-plane stresses are obtained by employing numerical schemes, such as finite differences, which may

not yield accurate results.

It is also important to verify the derivatives of in-plane stresses when modeling variable-stiffness composite structures. Because the material properties vary spatially in VS laminates, implying the variability of Hooke's coefficients at element level, the derivatives of material stiffness coefficients must be taken into account. For instance, to recover transverse shear stress τ_{yz} using Eq. (36), derivatives of in-plane stresses are calculated as

$$\begin{aligned}
\frac{\partial \tau_{xy}}{\partial x} &= \left(\bar{C}_{61}\frac{\partial \varepsilon_{xx}}{\partial x} + \bar{C}_{62}\frac{\partial \varepsilon_{yy}}{\partial x} + \bar{C}_{63}\frac{\partial \varepsilon_{zz}}{\partial x} + \bar{C}_{66}\frac{\partial \gamma_{xy}}{\partial x}\right) + \left(\varepsilon_{xx}\frac{\partial \bar{C}_{61}}{\partial x} + \varepsilon_{yy}\frac{\partial \bar{C}_{62}}{\partial x} + \varepsilon_{zz}\frac{\partial \bar{C}_{63}}{\partial x} + \gamma_{xy}\frac{\partial \bar{C}_{66}}{\partial x}\right), \\
\frac{\partial \sigma_{yy}}{\partial y} &= \left(\bar{C}_{21}\frac{\partial \varepsilon_{xx}}{\partial y} + \bar{C}_{22}\frac{\partial \varepsilon_{yy}}{\partial y} + \bar{C}_{23}\frac{\partial \varepsilon_{zz}}{\partial y} + \bar{C}_{26}\frac{\partial \gamma_{xy}}{\partial y}\right) + \left(\varepsilon_{xx}\frac{\partial \bar{C}_{21}}{\partial y} + \varepsilon_{yy}\frac{\partial \bar{C}_{22}}{\partial y} + \varepsilon_{zz}\frac{\partial \bar{C}_{23}}{\partial y} + \gamma_{xy}\frac{\partial \bar{C}_{26}}{\partial y}\right).
\end{aligned} \tag{37}$$

The derivatives of material stiffness coefficients can be computed exactly as given in Ref. [29] or by employing finite differences.

III. Numerical Results and Discussion

In this section, the three models discussed so far, namely UF-LW, UF-MZZF and UF-RZT, are employed for analyzing constant- and variable-stiffness composite laminates—labeled A–F. Through-thickness axial and transverse stresses are compared with 3D elasticity and 3D FE solutions as given in the literature [22, 33]. The material properties and stacking sequences for constant- and variable-stiffness laminates considered herein are tabulated in Tables 1, 2 and 3, respectively.

All results for axial normal, σ_{yy}, transverse shear, τ_{yz}, and transverse normal, σ_{zz}, stress presented in this paper are normalized as follows

$$\bar{\sigma}_{yy} = \frac{h^2}{q_0 L^2}\cdot\sigma_{yy}(x,y,z), \quad \bar{\tau}_{yz} = \frac{1}{q_0}\cdot\tau_{yz}(x,y,z), \quad \bar{\sigma}_{zz} = \frac{1}{q_0}\cdot\sigma_{zz}(x,y,z), \tag{38}$$

where h is the total laminate thickness, L is the beam length and q_0 is the applied loading magnitude.

A. Constant-Stiffness Composite Laminates

Consider a multilayered, square cross-section beam of length-to-thickness ratio, $L/h = 8$. The beam is aligned with the Cartesian y-axis and the cross-section is in the xz-plane. The layers are arranged in a general fashion with different ply thicknesses, material properties and material orientations. The beam is simply-supported at the two ends $y = 0$ and $y = L$ and loaded by a sinusoidal distributed load equally divided between the top and the bottom surfaces, $\mathrm{P}_z^{\mathrm{t}} = \mathrm{P}_z^{\mathrm{b}} = -q_0/2\cdot\sin(\pi y/L)$, as shown in Figure 2. Results obtained using the present approach are validated against Pagano's closed-form 3D elasticity solution [42]. As the exact solution is available for an infinitely wide plate subject to cylindrical bending [33], in the present approach, a plane strain condition is enforced. To realize this condition, material

Table 1 Mechanical properties of the materials considered in the present study.

Material	E_x	E_y	E_z	G_{yz}	G_{xz}	G_{xy}
	[GPa]					
p (carbon-fibre reinforced plastic)	1.0	25.0	1.0	0.5	0.2	0.5
pvc (poly-vinyl chloride foam)	0.25	0.25	0.25	0.0962	0.0962	0.0962
h (honey-comb)	0.25×10^{-3}	0.25×10^{-3}	2.5×10^{-3}	0.875×10^{-3}	1.75×10^{-3}	1.0×10^{-6}
IM7 (IM7/8852 composite)	12.0	163.0	12.0	4.0	3.2	5.0

	ν_{yz}	ν_{xz}	ν_{xy}
p	0.25	0.25	0.01
pvc	0.3	0.3	0.3
h	3.0×10^{-5}	3.0×10^{-5}	0.9
IM7	0.3	0.3	0.022

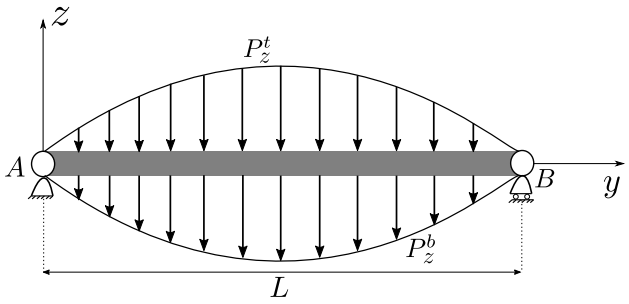

Fig. 2 Representation of a multilayered beam simply-supported at both the ends subjected to a sinusoidal distributed load at the top and the bottom surface.

stiffness coefficients $\bar{C}_{12}$, $\bar{C}_{13}$, $\bar{C}_{14}$, $\bar{C}_{15}$, $\bar{C}_{16}$, $\bar{C}_{24}$, $\bar{C}_{25}$, $\bar{C}_{26}$, $\bar{C}_{34}$, $\bar{C}_{35}$, $\bar{C}_{36}$, $\bar{C}_{45}$, $\bar{C}_{46}$ and $\bar{C}_{56}$ in Eq. (34) are all set to zero, as described in Appendix A of [40].

Layer-wise stresses are usually computed using the constitutive relation as given by Eq. (33). However, if the modeling fidelity is not sufficient most displacement-based approaches produce discontinuous transverse stresses at the layer interfaces, which violates the traction equilibrium condition between layers. The accuracy of the transverse stresses evaluated via Hooke's law is not acceptable when ESL models are employed. Moreover, transverse stresses calculated by integration of the equilibrium equations were shown to provide, in general, the best overall results, as

Table 2 Stacking sequence for constant-stiffness laminates considered in the present study. Subscripts indicate the repetition of a property over the corresponding number of layers.

Laminate	Layer thickness ratio	Material	Stacking sequence
Lam A	$[0.2_5]$	$[p_5]$	[90/0/90/0/90]
Lam B	$[0.1_2/0.2_3/0.1_2]$	$[p_2/pvc/h/pvc/p_2]$	$[90/0_5/90]$

also confirmed in [29]. For this reason, the in-plane stresses are herein calculated by using Hooke's law, whereas the transverse stresses are obtained via integration of the equilibrium equations.

The analyses are carried out by employing the LW and ESL theories within the UF-SLE framework. The beam is discretized with 30 B4 (four-noded) elements and a fifth-order expansion function is used to define cross-section kinematics. The number of beam elements and order of expansion are determined by performing a convergence analysis. Through-thickness distribution of normalized axial stress $\bar{\sigma}_{yy}$ (at $y = L/2$), transverse shear stress $\bar{\tau}_{yz}$ (at $y = 0$) and transverse normal stress $\bar{\sigma}_{zz}$ (at $y = L/2$) for laminates A and B are plotted in Figure 3. From the plots, it can be clearly seen that the LW approach of the UF-SLE model (UF-LW) shows excellent correlation with Pagano's 3D elasticity solution, as given in [22]. Moreover, the current fidelity of the model (with 30 B4 beam elements and fifth-order expansion) is sufficient to capture the transverse shear and normal stress profile accurately without any *posteriori* stress recovery step. For the ESL models with MZZF and RZT ZZ function, on the other hand, there is a need to recover the transverse stresses from the 3D stress equilibrium equations. However, a much greater gain in computational efficiency is obtained with the UF-MZZF and UF-RZT compared to the UF-LW model, as shown in Table 4, where the number of beam and cross-section elements, order of expansion, degrees of freedom (DOFs) and algebraic system complexities, for each case are compared. The recovered stress distributions are shown as UF-MZZF-SR and UF-RZT-SR in the plots. Clearly, for laminate A, both ESL models, UF-MZZF and UF-RZT, predict the stress response accurately. However, the UF-RZT model outperforms the UF-MZZF model in capturing the extreme case of transverse orthotropy in laminate B. This stress distribution arises due to the low transverse shear stiffness of the inner layer which makes it insufficient to support the peak transverse shear stress of the adjacent outer layer, and thus, a stress reversal in stiffer layers occurs.

B. Variable-Stiffness Composite Laminates

Consider a beam with length-to-thickness ratio $L/h = 10$, comprising N_l variable-stiffness composite layers. The beam, aligned with the Cartesian y-axis, is clamped at both ends $y = 0$ and $y = L$ and is assumed to undergo static deformations in plane strain under a uniformly distributed load equally divided between the top and the bottom surfaces $\mathrm{P}_z^{\mathrm{t}} = \mathrm{P}_z^{\mathrm{b}} = -q_0/2$, as shown in Figure 4. In this work, laminates with linear fiber angle variation along the beam axis and constant stiffness properties across the width are considered. The angle variation along the spanwise direction y of each ply k is defined using the notation of Gürdal and Olmedo [43],

$$\theta^{(k)}(y) = \frac{2(T_1^{(k)} - T_0^{(k)})}{L} \left| y - \frac{L}{2} \right| + T_0^{(k)}, \tag{39}$$

where $\theta^{(k)}(y)$ is the local fiber angle at co-ordinate y, and $T_0^{(k)}$ and $T_1^{(k)}$, written as $\langle T_0^{(k)} | T_1^{(k)} \rangle$, are the fiber angles at the beam midspan, $y = L/2$, and ends, $y = 0, L$, respectively. Hence, the fiber angle in each ply takes the value $T_1^{(k)}$ at one end of the beam, is steered to $T_0^{(k)}$ at the mid-span and then returns to $T_1^{(k)}$ at the other end of the beam.

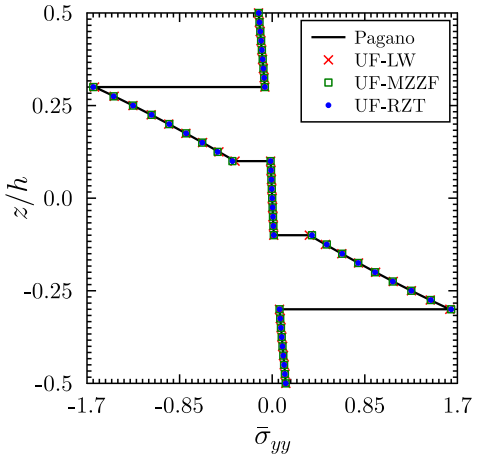

(a) Lam A: $\bar{\sigma}_{yy}$ at $y = L/2$

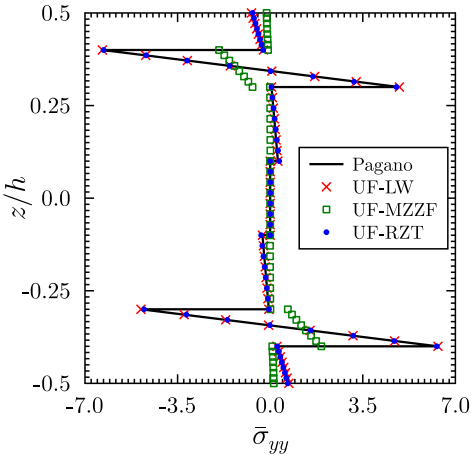

(b) Lam B: $\bar{\sigma}_{yy}$ at $y = L/2$

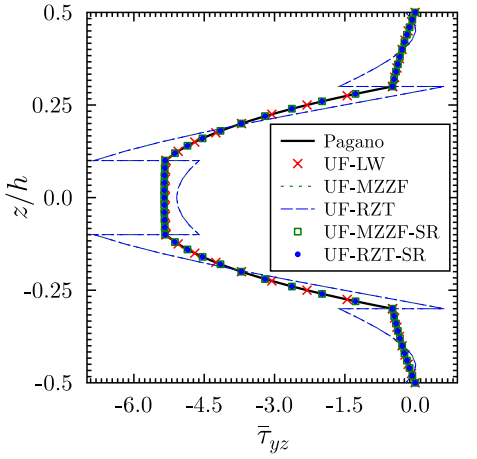

(c) Lam A: $\bar{\tau}_{yz}$ at $y = 0$

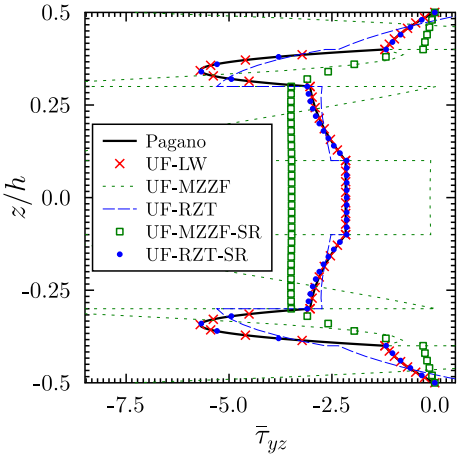

(d) Lam B: $\bar{\tau}_{yz}$ at $y = 0$

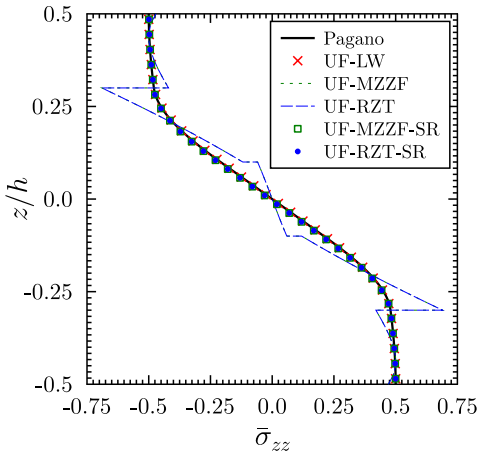

(e) Lam A: $\bar{\sigma}_{zz}$ at $y = L/2$

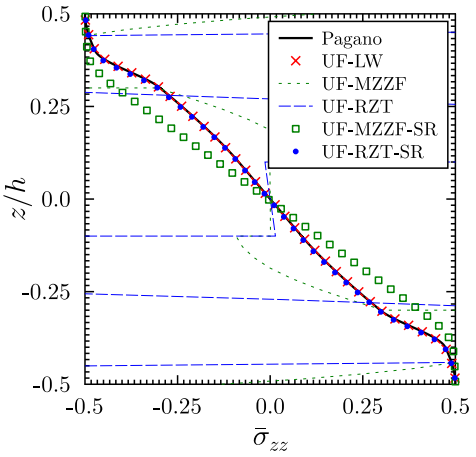

(f) Lam B: $\bar{\sigma}_{zz}$ at $y = L/2$

Fig. 3 Through-thickness distribution of the normalized axial, transverse shear and transverse normal stresses for laminates A and B.

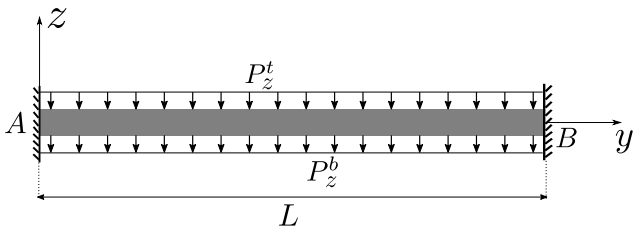

Fig. 4 Representation of a multilayered beam clamped at both the ends subjected to a uniformly distributed load on the top and the bottom surfaces.

Table 3 Stacking sequence for variable-stiffness laminates considered in the present study. Subscripts indicate the repetition of a property over the corresponding number of layers.

Laminate	Layer thickness ratio	Material	Stacking sequence $\langle T_0 \vert T_1 \rangle$
VS Lam C	$[(1/8)_8]$	$[IM7_8]$	$[\langle 90\vert 0\rangle/\langle -90\vert 0\rangle/\langle 45\vert -45\rangle/\langle -45\vert 45\rangle]_s$
VS Lam D	$[(1/12)_4/(1/3)/(1/12)_4]$	$[p_4/pvc/p_4]$	$[\langle 0\vert 90\rangle/\langle 90\vert 0\rangle/\langle 0\vert -90\rangle/\langle -90\vert 0\rangle/...$ $0/\langle -90\vert 0\rangle/\langle 0\vert -90\rangle/\langle 90\vert 0\rangle/\langle 0\vert 90\rangle]$
VS Lam E	$[(1/8)_2/0.5/(1/8)_2]$	$[p_2/pvc/p_2]$	$[\langle 45\vert -45\rangle/\langle -45\vert 45\rangle/0/\langle -45\vert 45\rangle/\langle 45\vert -45\rangle]$
VS Lam F	$[(1/12)_4/(1/3)/(1/12)_4]$	$[p_4/pvc/p_4]$	$[\langle 20\vert -60\rangle/\langle -20\vert 60\rangle/\langle 45\vert -45\rangle/\langle -45\vert 45\rangle/...$ $0/0/90/\langle 35\vert -35\rangle/\langle -35\vert 35\rangle]$

The static analysis of VS beams C-F are performed using the LW and ESL theories within the UF-SLE model. The number of beam and cross-section elements, and the order of expansion function employed for each case is given in Table 4. To the authors' knowledge there are no 3D closed form solutions for variable-stiffness beams in bending. Therefore, the stress results obtained are verified against 3D Finite Element (FE) solutions, as given in Chapter 6 of [33], obtained using the commercial software package Abaqus. The 3D FE benchmark model in Abaqus featured a 250 mm long, 1000 mm wide and 25 mm thick plate that was meshed using a total of 95,880 linear C3D8R elements with 799 elements along the length, 120 elements throught the thickness, and a single element across the width. Figures 5 and 6 show through-thickness plots of in-plane normal stress $\bar{\sigma}_{yy}$ at the mid-span of the beam, transverse shear stress $\bar{\tau}_{yz}$ at the quarter-span of the beam and transverse normal stress $\bar{\sigma}_{zz}$ at the mid-span of the beam for VS laminates C-F.

From these plots, it is evident that the stress distribution obtained using the LW approach is in excellent agreement with the 3D FE solution. The axial normal $\bar{\sigma}_{yy}$ and transverse shear $\bar{\tau}_{yz}$ stress distribution obtained using the ESL model (UF-MZZF) correlates well with 3D FE for VS laminates C, D and E, whereas for the arbitrary sandwich beam, VS laminate F, significant differences are observed (Figures 6b and 6d). These differences show the inability of MZZF in capturing the zig-zag effect accurately for highly heterogeneous sandwich beams. In contrast, the UF-RZT model predicts the stress response accurately for all variable-stiffness laminates considered herein and results are in close agreement with 3D FE solutions. However, from the transverse normal stress $\bar{\sigma}_{zz}$ plots, it seems that both ZZ models are

unable to capture the thickness stretching effect for VS laminates C, E and F. The reason for this disparity is the presence of an absolute value in the function used to describe the fiber orientation (Eq. (39)), which leads to a discontinuity in fiber angle slope and curvature. This discontinuity, in turn, results in a continuous but non-differentiable distribution of transverse shear stress $\bar{\tau}_{yz}$ at the mid-span. Thus, the UF-MZZF and the UF-RZT models predict an incorrect $\bar{\sigma}_{zz}$ distribution as it is recovered from Cauchy's equilibrium equation, described in Section IIE. On the other hand, the UF-LW model is able to predict the transverse stress results accurately as these are computed directly from the underlying constitutive equations. For VS laminate D, since all layers have fiber orientation angle (T_0) value at the mid-span with either 0° or 90°, the transverse shear stress distribution is continuous and differentiable, and therefore, the transverse normal stress correlates well for all models as shown in Figure 5f. The reader is referred to the authors' previous work [35] for more insight on these intricacies in modeling variable-stiffness laminates.

To check the applicability of proposed models (UF-MZZF and UF-RZT) at locations along the beam other than the fiber angle singularity (mid-span in the present case), through-thickness distributions of $\bar{\sigma}_{yy}$, $\bar{\tau}_{yz}$ and $\bar{\sigma}_{zz}$ are plotted at $y = 0.1L$ and $0.2L$, for VS laminates C, E and F, in Figures 7 to 9. It can be clearly seen that the results obtained using the UF-RZT model is in excellent agreement with the UF-LW model for all the VS laminates, even near the boundary. The UF-MZZF model is accurate for VS laminates C and E, but fails to capture the zig-zag effect and a reversal in transverse shear stress profile intensified by the clamped support condition in VS sandwich laminate F. Furthermore, it is to be noted that this is the first time that RZT is used within a hierarchical displacement-based model to analyze variable-stiffness beams. Previously, Groh and Weaver [33] used the RZT ZZ function within the Hellinger-Reissner mixed formulation to model variable-stiffness beams. It was observed that due to the dependence of the RZT ZZ function on transverse shear rigidities, the ZZ effect can vanish in some areas of the beam and this vanishing ZZ effect leads to numerical instabilities in the model. This is not the case with the present Serendipity Lagrange finite element model because, in contrast to the work by Groh & Weaver, the mathematical domain is decomposed into smaller subdomains with local support (finite elements) rather than one domain with global support. Moreover, the UF-SLE ESL approach is computationally more efficient than the 3D FE and the UF-LW model, as shown in Table 4. However, the UF-LW model can be a viable alternative in cases where 3D Finite Element (FE) analysis is required due to the presence of very localized stress gradients or layer-wise boundary conditions.

IV. Conclusion

In the authors' previous work [35, 40], the displacement-based Unified Formulation model, based on the hierarchical Serendipity Lagrange Expansion finite element (UF-SLE), was used to derive a Layer-Wise model for constant- and variable-stiffness beams. In this work, to reduce the computational expense, an Equivalent Single Layer approach is implemented within the UF-SLE framework. To account for the ZZ effect, Murakami's Zig-Zag Function (MZZF) and Refined Zig-Zag Theory (RZT) functions are used to model constant- and variable-stiffness laminated and sandwich

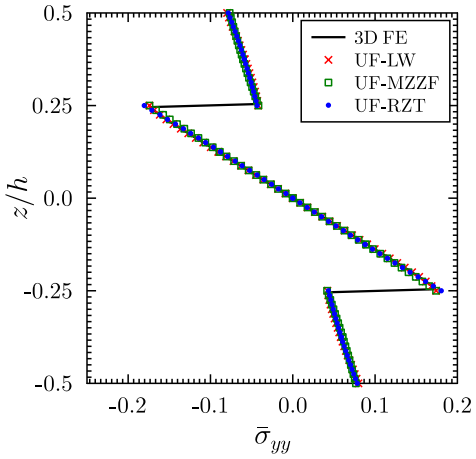

(a) VS Lam C: $\bar{\sigma}_{yy}$ at $y = L/2$

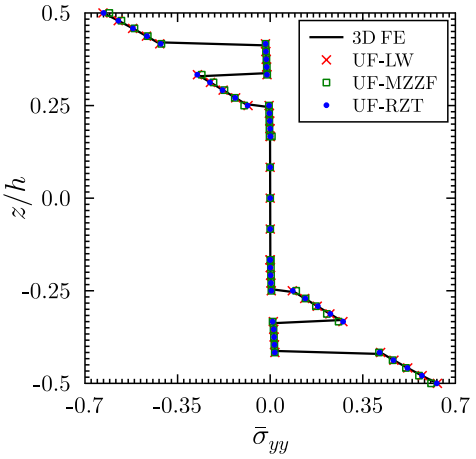

(b) VS Lam D: $\bar{\sigma}_{yy}$ at $y = L/2$

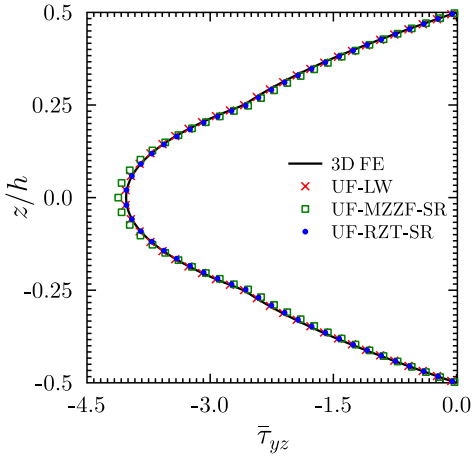

(c) VS Lam C: $\bar{\tau}_{yz}$ at $y = L/4$

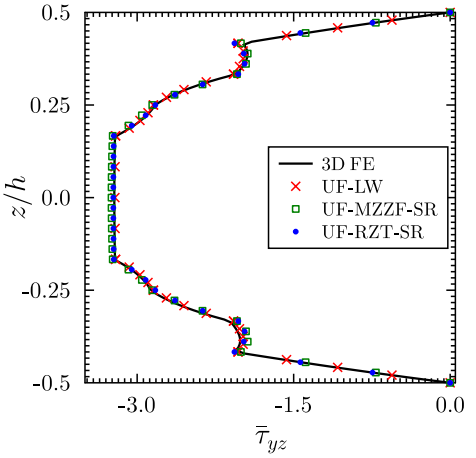

(d) VS Lam D: $\bar{\tau}_{yz}$ at $y = L/4$

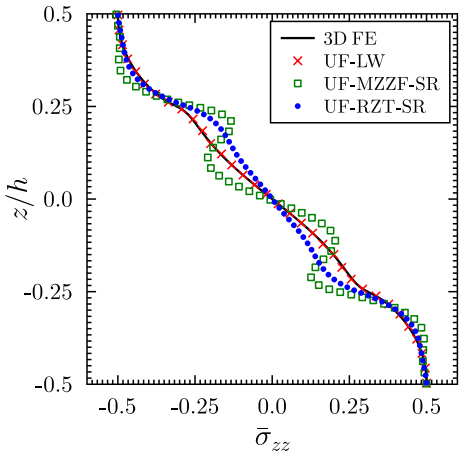

(e) VS Lam C: $\bar{\sigma}_{zz}$ at $y = L/2$

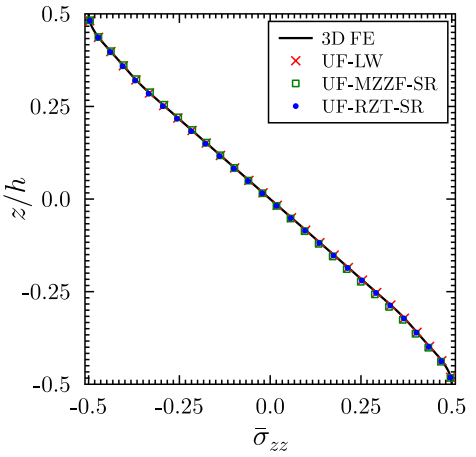

(f) VS Lam D: $\bar{\sigma}_{zz}$ at $y = L/2$

Fig. 5 Through-thickness distribution of the normalized axial and transverse shear stresses for variable-stiffness laminates C.

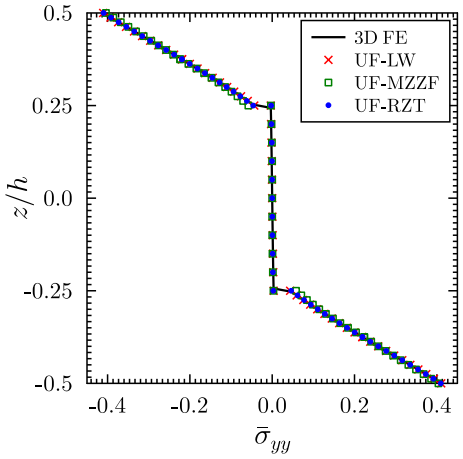

(a) VS Lam E: $\bar{\sigma}_{yy}$ at $y = L/2$

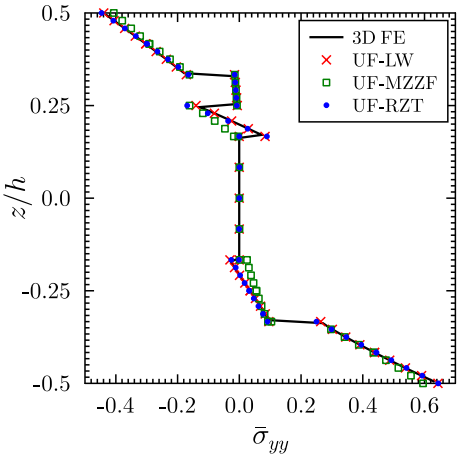

(b) VS Lam F: $\bar{\sigma}_{yy}$ at $y = L/2$

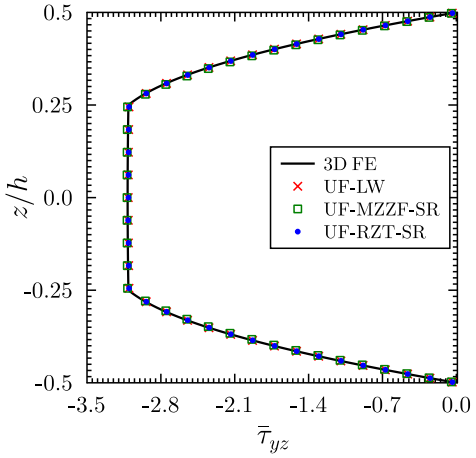

(c) VS Lam E: $\bar{\tau}_{yz}$ at $y = L/4$

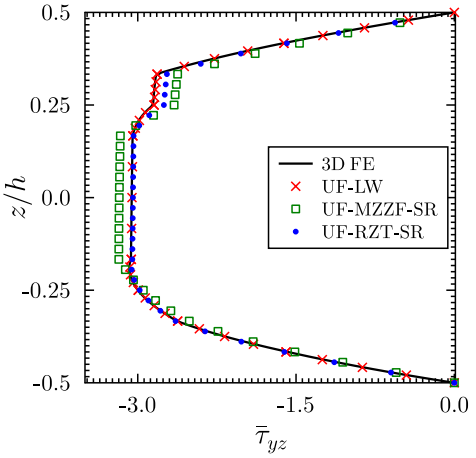

(d) VS Lam F: $\bar{\tau}_{yz}$ at $y = L/4$

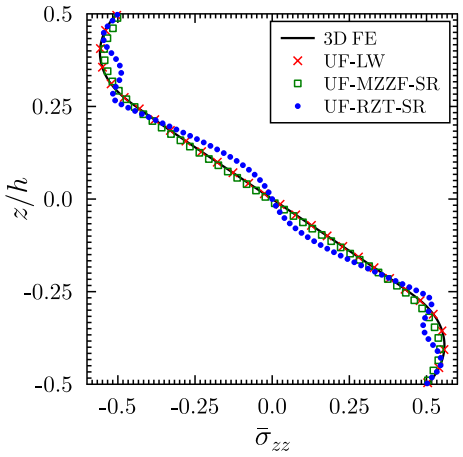

(e) VS Lam E: $\bar{\sigma}_{zz}$ at $y = L/2$

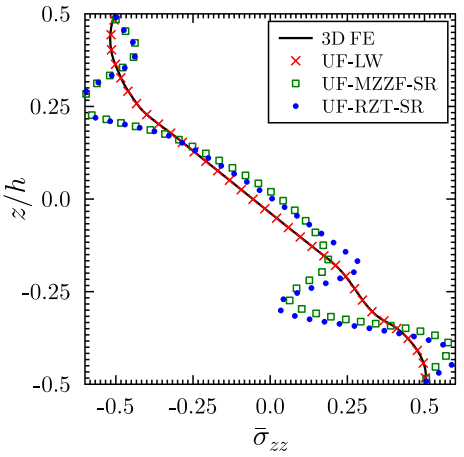

(f) VS Lam F: $\bar{\sigma}_{zz}$ at $y = L/2$

Fig. 6 Through-thickness distribution of the normalized axial and transverse shear stresses for variable-stiffness laminates E.

Table 4 Comparison of number of beam elements (Y), Serendipity Lagrange (SL) cross-section elements (Z), expansion order (N), DOFs (n) and computational complexities (O) associated with each model.

Model	Y **B4**	Z **SL**N	**DOFs** n	**Time*** $\sim O(n^2)$	**Space*** $\sim O(nb^{**})$	Y **B4**	Z **SL**N	**DOFs** n	**Time** $\sim O(n^2)$	**Space** $\sim O(nb)$
	Lam A					**Lam B**				
UF-LW	30 B4	5 SL5	24,843	10^8	10^7	30 B4	7 SL5	34,125	10^9	10^7
UF-MZZF	30 B4	1 SL5	6,825	10^7	10^6	30 B4	1 SL5	6,825	10^7	10^6
UF-RZT	30 B4	1 SL5	6,825	10^7	10^6	30 B4	1 SL5	6,825	10^7	10^6
	VS Lam C					**VS Lam D**				
3D FE [33]	-	-	580,800	10^{11}	10^7	-	-	580,800	10^{11}	10^7
UF-LW	40 B4	8 SL4	36,663	10^9	10^7	40 B4	9 SL4	41,019	10^9	10^7
UF-MZZF	50 B4	1 SL5	10,721	10^8	10^6	40 B4	1 SL5	8,591	10^7	10^6
UF-RZT	50 B4	1 SL5	10,721	10^8	10^6	40 B4	1 SL5	8,591	10^7	10^6
	VS Lam E					**VS Lam F**				
3D FE [33]	-	-	580,800	10^{11}	10^7	-	-	580,800	10^{11}	10^7
UF-LW	40 B4	5 SL4	23,595	10^8	10^7	40 B4	9 SL4	41,019	10^9	10^7
UF-MZZF	50 B4	1 SL5	10,721	10^8	10^6	70 B4	1 SL6	19,412	10^8	10^6
UF-RZT	50 B4	1 SL5	10,721	10^8	10^6	70 B4	1 SL6	19,412	10^8	10^6

*Time and space complexities associated with a pre-conditioner conjugate gradient algorithm (iterative solver) [40, 44].
**b denotes the bandwidth of a matrix.

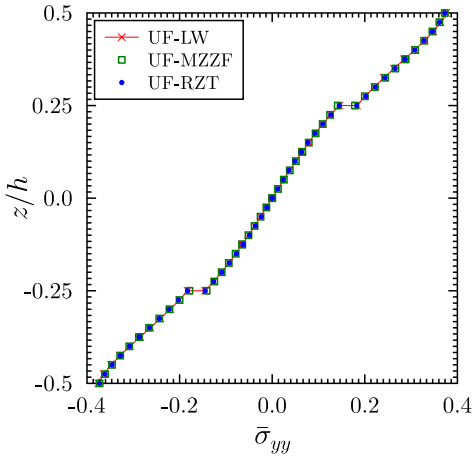

(a) VS Lam C: $\bar{\sigma}_{yy}$ at $y = 0.1L$

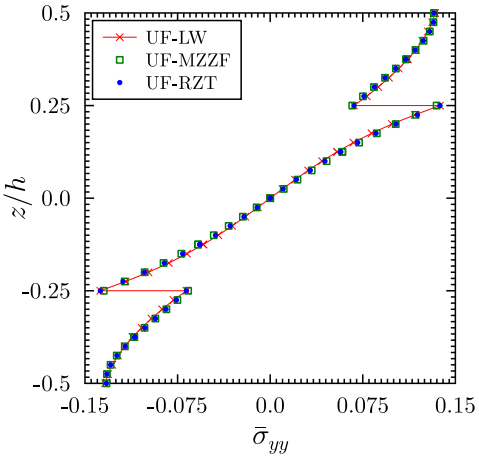

(b) VS Lam C: $\bar{\sigma}_{yy}$ at $y = 0.2L$

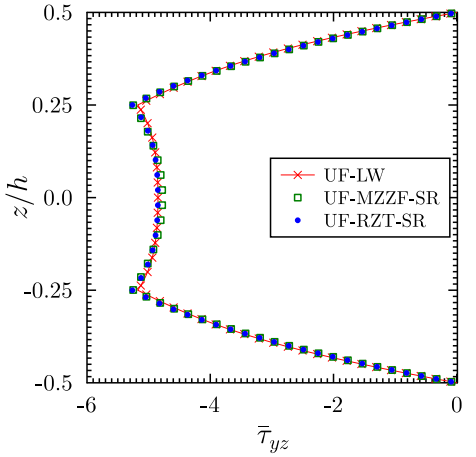

(c) VS Lam C: $\bar{\tau}_{yz}$ at $y = 0.1L$

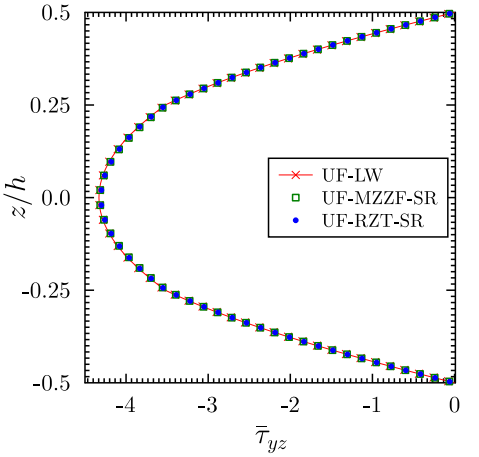

(d) VS Lam C: $\bar{\tau}_{yz}$ at $y = 0.2L$

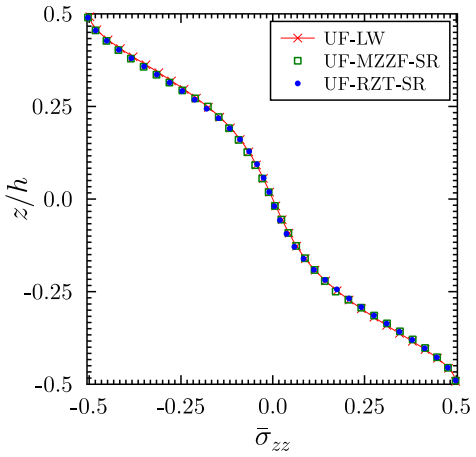

(e) VS Lam C: $\bar{\sigma}_{zz}$ at $y = 0.1L$

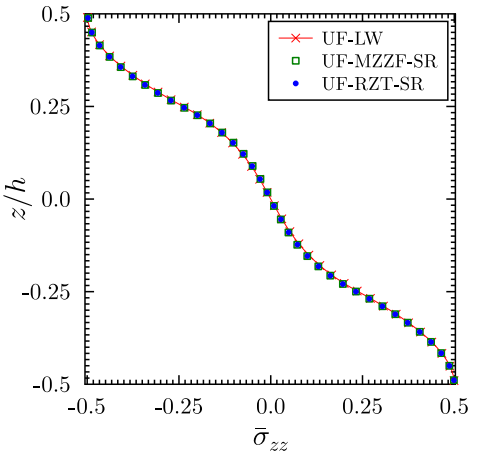

(f) VS Lam C: $\bar{\sigma}_{zz}$ at $y = 0.2L$

Fig. 7 Through-thickness distribution of the normalized axial and transverse stresses, at 10% and 20% of the beam length from the clamped end, for variable-stiffness laminate C.

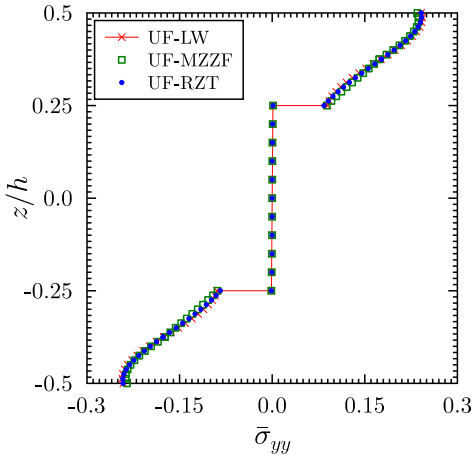

(a) VS Lam E: $\bar{\sigma}_{yy}$ at $y = 0.1L$

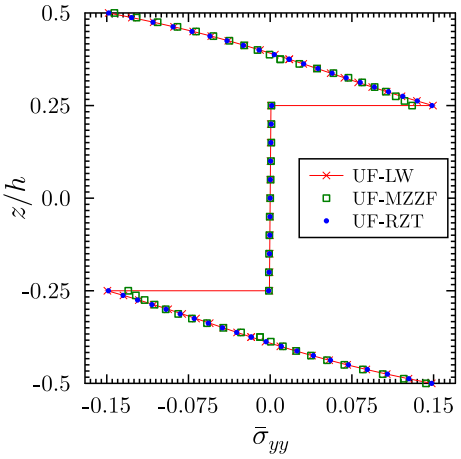

(b) VS Lam E: $\bar{\sigma}_{yy}$ at $y = 0.2L$

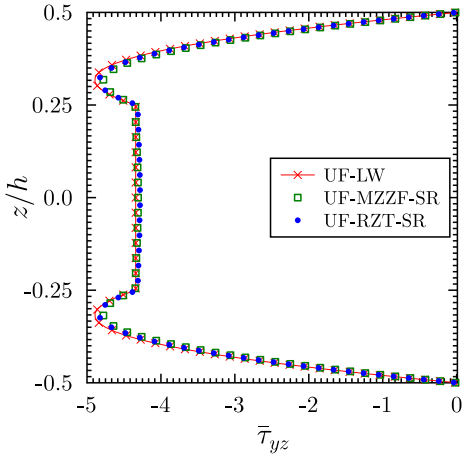

(c) VS Lam E: $\bar{\tau}_{yz}$ at $y = 0.1L$

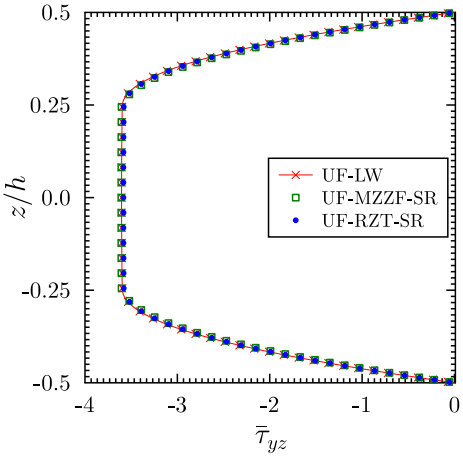

(d) VS Lam E: $\bar{\tau}_{yz}$ at $y = 0.2L$

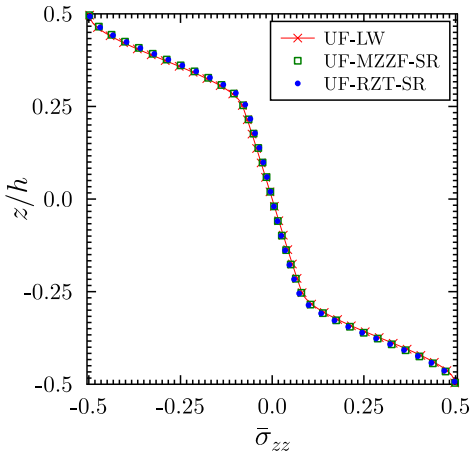

(e) VS Lam E: $\bar{\sigma}_{zz}$ at $y = 0.1L$

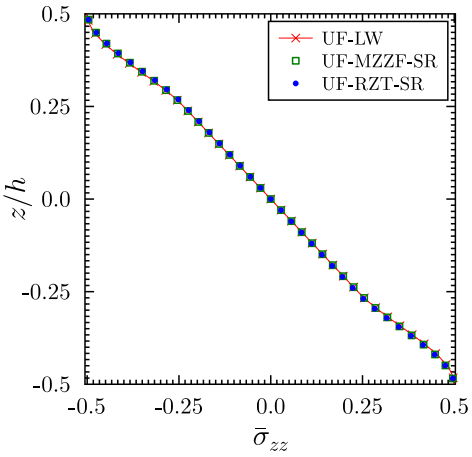

(f) VS Lam E: $\bar{\sigma}_{zz}$ at $y = 0.2L$

Fig. 8 Through-thickness distribution of the normalized axial and transverse stresses, at 10% and 20% of the beam length from the clamped end, for variable-stiffness laminate E.

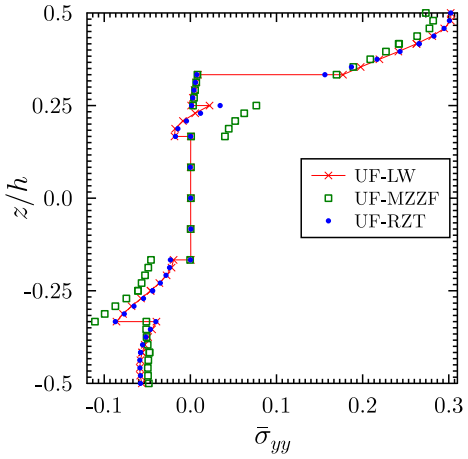

(a) VS Lam F: $\bar{\sigma}_{yy}$ at $y = 0.1L$

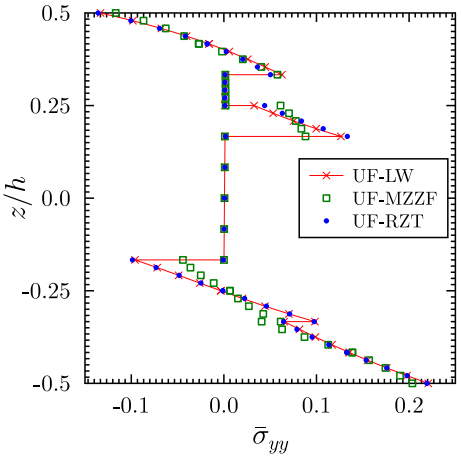

(b) VS Lam F: $\bar{\sigma}_{yy}$ at $y = 0.2L$

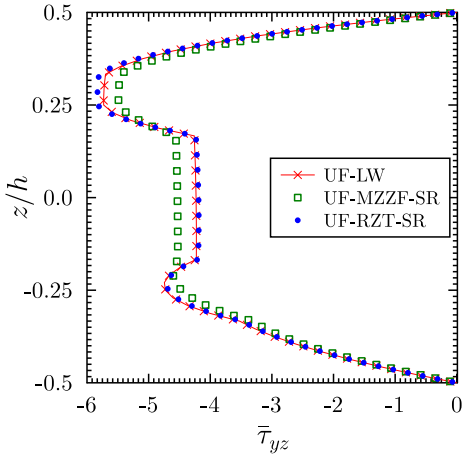

(c) VS Lam F: $\bar{\tau}_{yz}$ at $y = 0.1L$

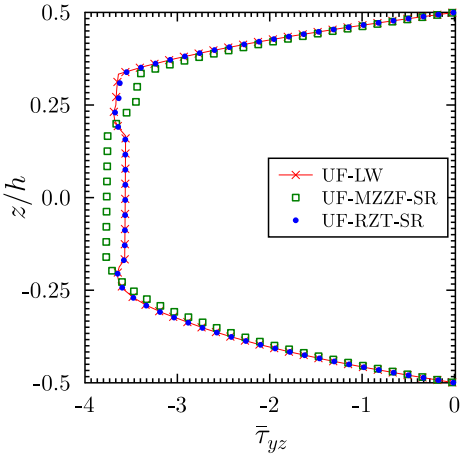

(d) VS Lam F: $\bar{\tau}_{yz}$ at $y = 0.2L$

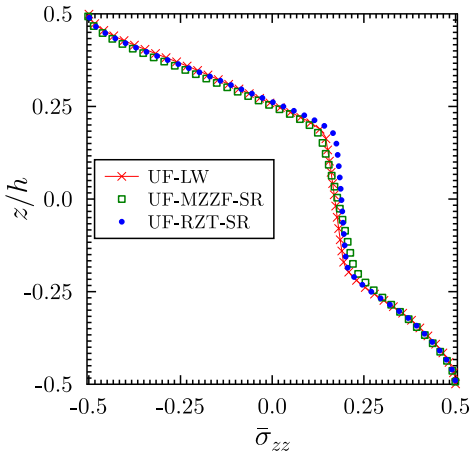

(e) VS Lam F: $\bar{\sigma}_{zz}$ at $y = 0.1L$

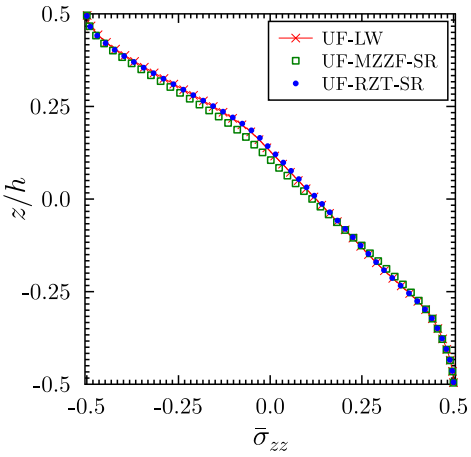

(f) VS Lam F: $\bar{\sigma}_{zz}$ at $y = 0.2L$

Fig. 9 Through-thickness distribution of the normalized axial and transverse stresses, at 10% and 20% of the beam length from the clamped end, for variable-stiffness laminate F.

beams. The continuous distribution of transverse stresses across the layers is obtained *a posteriori* by integrating the in-plane stresses in Cauchy's 3D indefinite equilibrium equations. The UF-MZZF model is shown to be insufficient in capturing the stress response accurately for highly heterogeneous sandwich beams. On the other hand, the UF-RZT model predicts the three-dimensional (3D) stress response accurately for all cases considered herein, and is shown to be more computationally efficient than the UF-SLE layer-wise model (UF-LW) and the 3D finite element (FE) model. Thus, the combination of accuracy and computational expense makes this approach an attractive basis for industrial design tools. However, the UF-LW model is still preferred over the UF-RZT model in the presence of localized stress gradients or mathematical singularities in the constitutive relations, which can be observed for variable-stiffness composites.

Acknowledgements

This research has been developed in the framework of the FULLCOMP project, supported by the H2020 Marie Skłodowska-Curie European Training Network [Grant No. 642121]. Alberto Pirrera is funded by the EPSRC [Grant No. EP/M013170/1]. Rainer Groh is supported by the Royal Academy of Engineering under the Research Fellowship scheme [Grant No. RF\201718\17178]. Paul M. Weaver would like to acknowledge the support of the Royal Society for the Royal Society Wolfson Merit and the Science Foundation Ireland for the award of a Research Professor grant (Varicomp: 15/RP/2773).

References

[1] Everstine, G., and Pipkin, A., "Stress channelling in transversely isotropic elastic composites," *Zeitung fuer angewandte Mathematik und Physik (ZAMP)*, Vol. 22, 1971, pp. 825 – 834. doi:10.1007/BF01591811.

[2] di Sciuva, M., "A refinement of the transverse shear deformation theory for multilayered orthotropic plates," *L'aerotecnica missile e spazio*, Vol. 62, 1984, pp. 84–92.

[3] Lozano, G. G., Tiwari, A., Turner, C., and Astwood, S., "A review on design for manufacture of variable stiffness composite laminates," *Journal of Engineering Manufacture*, Vol. 230, 2016, pp. 981 – 992. doi:10.1177/0954405415600012.

[4] Jones, R. M., *Mechanics of Composite Materials*, Taylor & Francis Ltd., London, UK, 1998.

[5] Mindlin, R. D., "Influence of rotary inertia and shear on flexural motion of isotropic elastic plates," *Journal of Applied Mechanics*, Vol. 18, 1951, pp. 31–38.

[6] Levinson, M., "A new rectangular beam theory," *Journal of Sound and Vibration*, Vol. 74, 1981, pp. 81–87. doi:10.1016/0022-460X(81)90493-4.

[7] Reddy, J. N., "A Simple Higher-Order Theory for Laminated Composite Plates," *Journal of Applied Mechanics*, Vol. 51, 1984, pp. 745–752. doi:10.1115/1.3167719.

[8] Lo, K., Christensen, R., and Wu, E., "A High-Order Theory of Plate Deformation - Part 2: Laminated Plates," *Journal of Applied Mechanics*, Vol. 44 (4), 1977, pp. 669–676. doi:10.1115/1.3424155.

[9] Seide, P., "XXIX - An Improved Approximate Theory for the Bending of Laminated Plates," *Mechanics Today*, Vol. 5, 1980, pp. 451–466. doi:10.1016/B978-0-08-024249-1.50039-X.

[10] Carrera, E., "Historical review of Zig-Zag theories for multilayered plates and shells," *Applied Mechanics Review*, Vol. 56, 2003, pp. 287–308. doi:10.1115/1.1557614.

[11] Icardi, U., and Sola, F., "Assessment of recent zig-zag theories for laminated and sandwich structures," *Composites Part B: Engineering*, Vol. 97, 2016, pp. 26–52. doi:10.1016/j.compositesb.2016.04.058.

[12] Murakami, H., "Laminated composite plate theory with improved in-plane responses," *Journal of Applied Mechanics*, Vol. 53, 1986, pp. 661 – 666. doi:10.1115/1.3171828.

[13] Carrera, E., "Developments, ideas and evaluations based upon Reissner's mixed variational theorem in the modeling of multilayered plates and shells," *Composite Structures*, Vol. 37, 1997, pp. 373–383. doi:10.1115/1.1385512.

[14] Carrera, E., "On the use of the Murakami's zig-zag function in the modeling of layered plates and shells," *Computers and Structures*, Vol. 82, 2004, pp. 541 – 554. doi:10.1016/j.compstruc.2004.02.006.

[15] Brischetto, S., Carrera, E., and Demasi, L., "Improved bending analysis of sandwich plates using zig-zag functions," *Composite Structures*, Vol. 89, 2009, pp. 408 – 415. doi:10.1016/j.compstruct.2008.09.001.

[16] Demasi, L., "Refined Multilayered Plate Elements Based on Murakami Zig-Zag Function," *Composite Structures*, Vol. 70, 2005, pp. 308 – 316. doi:10.1016/j.compstruct.2004.08.036.

[17] Ganapathi, M., Patel, B. P., and Pawargi, D. S., "Dynamic Analysis of Laminated Cross-Ply Composite Non-Circular Thick Cylindrical Shells Using Higher-Order Theory," *International Journal of Solids and Structures*, Vol. 39, 2002, pp. 5945 – 5962. doi:10.1016/S0020-7683(02)00495-X.

[18] Demasi, L., "2D, Quasi 3D and 3D Exact Solutions for Bending of Thick and Thin Sandwich Plates," *Journal of Sandwich Structures and Materials*, Vol. 10, 2008, pp. 271 – 310. doi:10.1177/1099636208089311.

[19] Gherlone, M., "On the Use of Zigzag Functions in Equivalent Single Layer Theories for Laminated Composite and Sandwich Beams: A Comparative Study and Some Observations on External Weak Layers," *Journal of Applied Mechanics*, Vol. 80, 2013, pp. JAM–12–1229. doi:10.1115/1.4023690.

[20] Tessler, A., di Sciuva, M., and Gherlone, M., "Refinement of Timoshenko beam theory for composite and sandwich beams using zigzag kinematics," *National Aeronautics and Space Administration*, Vol. 215086, 2007.

[21] Tessler, A., di Sciuva, M., and Gherlone, M., "A Refined Zigzag Beam Theory for Composite and Sandwich Beams," *Journal of Composite Materials*, Vol. 43, 2009, pp. 1051–1081. doi:10.1177/0021998308097730.

[22] Groh, R. M. J., and Weaver, P. M., "On displacement-based and mixed-variational equivalent single layer theories for modelling highly heterogeneous laminated beams," *International Journal of Solids and Structures*, Vol. 59, 2015, pp. 147–170. doi:10.1016/j.ijsolstr.2015.01.020.

[23] Groh, R. M. J., and Tessler, A., "Computationally efficient beam elements for accurate stresses in sandwich laminates and laminated composites with delaminations," *Computer Methods in Applied Mechanics and Engineering*, Vol. 320, 2017, pp. 369–395. doi:10.1016/j.cma.2017.03.035.

[24] Xin, Z., Duan, Y., Xu, W., Zhang, T., and Wang, B., "Review of the mechanical performance of variable stiffness design fiber-reinforced composites," *Science and Engineering of Composite Materials*, Vol. 25(3), 2016, pp. 425 – 437. doi: 10.1515/secm-2016-0093.

[25] Langley, T., *Finite element modeling of tow-placed variable- stiffness composite laminates*, MSc thesis, Virginia Tech, Blacksburg, 1999.

[26] Soriano, A., and Díaz, J., "Failure analysis of variable stiffness composite plates using continuum damage mechanics models," *Composite Structures*, Vol. 184, 2018, pp. 1071 – 1080. doi:10.1016/j.compstruct.2017.10.065.

[27] Akhavan, H., Ribeiro, P., and de Moura, M. F. S. F., "Large deflection and stresses in variable stiffness composite laminates with curvilinear fibre," *International Journal of Mechanical Sciences*, Vol. 73, 2013, pp. 14 – 26. doi:10.1016/j.ijmecsci.2013.03.013.

[28] Tornabene, F., Fantuzzi, N., and Bacciocchi, M., "Higher-order structural theories for the static analysis of doubly-curved laminated composite panels reinforced by curvilinear fibers," *Thin-Walled Structures*, Vol. 102, 2016, pp. 222 – 245. doi:10.1016/j.tws.2016.01.029.

[29] Demasi, L., Biagini, G., Vannucci, F., Santarpia, E., and Cavallaro, R., "Equivalent Single Layer, Zig-Zag, and Layer Wise theories for variable angle tow composites based on the Generalized Unified Formulation," *Composite Structures*, Vol. 177, 2017, pp. 54 – 79. doi:10.1016/j.compstruct.2017.06.033.

[30] Demasi, L., "Hierarchy plate theories for thick and thin composite plates: The generalized unified formulation," *Composite Structures*, Vol. 84, 2008, pp. 256–270. doi:10.1016/j.compstruct.2007.08.004.

[31] Demasi, L., "Invariant Finite Element Model for Composite Structures: The Generalized Unified Formulation," *AIAA Journal*, Vol. 48, 2010, pp. 1602–1619. doi:10.2514/1.45416.

[32] Demasi, L., Ashenafi, Y., Cavallaro, R., and Santarpia, E., "Generalized Unified Formulation shell element for functionally graded Variable-Stiffness Composite Laminates and aeroelastic applications," *Composite Structures*, Vol. 131, 2015, pp. 501 – 515. doi:10.1016/j.compstruct.2015.05.022.

[33] Groh, R. M. J., *Non-classical effects in straight-fibre and tow-steered composite beams and plates*, PhD thesis, Department of Aerospace Engineering, University of Bristol, 2015.

[34] Groh, R. M. J., and Weaver, P. M., "A computationally efficient 2D model for inherently equilibrated 3D stress predictions in heterogeneous laminated plates. Part I: Model formulation," *Composite Structures*, Vol. 156, 2016, pp. 171–185. doi: 10.1016/j.compstruct.2015.11.078.

[35] Patni, M., Minera, S., Groh, R. M. J., Pirrera, A., and Weaver, P. M., "On the accuracy of localised 3D stress fields in tow-steered laminated composite structures," *submitted to Composite Structures*, February 2018.

[36] Carrera, E., Giunta, G., and Petrolo, M., *A Modern and Compact Way to Formulate Classical and Advanced Beam Theories*, Saxe-Coburg Publications, United Kingdom, 2010.

[37] Carrera, E., and Petrolo, M., "Refined One-Dimensional Formulations for Laminated Structure Analysis," *AIAA Journal*, Vol. 50, 2012, p. 176–189. doi:10.2514/1.J051219.

[38] Carrera, E., Pagani, A., and Petrolo, M., "Classical, Refined, and Component-Wise Analysis of Reinforced-Shell Wing Structures," *AIAA Journal*, Vol. 51, 2013, p. 1255–1268. doi:10.2514/1.J052331.

[39] Minera, S., Patni, M., Carrera, E., Petrolo, M., Weaver, P. M., and Pirrera, A., "Three-dimensional stress analysis for beam-like structures using Serendipity Lagrange shape functions," *International Journal of Solids and Structures*, Vol. 141-142, 2018, pp. 279–296. doi:10.1016/j.ijsolstr.2018.02.030.

[40] Patni, M., Minera, S., Groh, R. M. J., Pirrera, A., and Weaver, P. M., "Three-dimensional stress analysis for laminated composite and sandwich structures," *Composites Part B: Engineering*, Vol. 155, 2018, pp. 299–328. doi:10.1016/j.compositesb.2018.08.127.

[41] Reddy, J. N., *Mechanics of Laminated Composite Plates and Shells. Theory and Analysis, Second Edition*, CRC Press, 2004.

[42] Pagano, N. J., "Exact solutions for composite laminates in cylindrical bending," *Journal of Composite Materials*, Vol. 3(3), 1969, pp. 398–411. doi:10.1177/002199836900300304.

[43] Gürdal, Z., and Olmedo, R., "In-plane response of laminates with spatially varying fiber orientations: variable stiffness concept," *AIAA Journal*, Vol. 31(4), 1993, pp. 751 – 758. doi:10.2514/3.11613.

[44] Jiang, S., Yang, L., Alsoliby, S., and Zhou, G., "PCG solver and its computational complexity for implicit control-volume finite-element method of RTM mold filling simulation," *Composites Science and Technology*, Vol. 67, 2007, pp. 3316 – 3322. doi:10.1016/j.compscitech.2007.03.030.